Pharmacological Research 224 (2026) 108087

Contents lists available at ScienceDirect

Pharmacological Research

journal homepage: www.elsevier.com/locate/yphrs

FASN targeting by G28UCM impairs mitochondrial fatty acid synthesis and reveals a FASN–SDHB synthetic interaction

Nastasia Wilfinger-Lutz [a,1], Kristina M. Kuehrer [a,1], Maria J. Bueno [b], Michaela Schwaiger-Haber [c], Wen-An Wang [d], Katrin Krejci [a], Ronald Mekis [d], Nicolle Gobbo Oliveira Erünlü [d], Anne Miller [e], Alexandra Junza [f], Siegfried Reipert [g], Michael Bergmann [h], Oscar Yanes [f], Arvand Haschemi [e], Gunda Koellensperger [c], Miguel Quintela-Fandino [b,i,j], Karin Nowikovsky [a,d,*]

[a] Internal Medicine I, Medical University Vienna and Comprehensive Cancer Center, Austria
[b] Breast Cancer Clinical Research Unit, CNIO - Spanish National Cancer Research Center, Melchor Fernandez Almagro, Madrid, Spain
[c] Department of Analytical Chemistry and Vienna Metabolomics Center (VIME), University of Vienna, Austria
[d] Department of Biological Sciences, University of Veterinary Medicine Vienna, Austria
[e] Department of Laboratory Medicine (KILM), Medical University Vienna, Austria
[f] CIBER de Diabetes y Enfermedades Metabólicas Asociadas (CIBERDEM), Instituto de Salud Carlos III, and Universitat Rovira i Virgili, Department of Electronic Engineering & IISPV, Spain
[g] Core Facility Cell Imaging and Ultrastructure Research, University of Vienna, Austria
[h] Department of Visceral Surgery, Medical University Vienna, Austria
[i] Medical Oncology Hospital, Universitario Quiron, Pozuelo de Alarcon, Madrid, Spain
[j] Medical Oncology, Hospital Universitario de Fuenlabrada, Fuenlabrada, Madrid, Spain

ARTICLE INFO

Keywords:
FASN
mtFAS
SDHB
LIAS
Cancer
G28UCM

ABSTRACT

Metabolic reprogramming in cancer relies on lipid synthesis and mitochondrial function, yet how these processes, other than citrate flux and β-oxidation, intersect remains unclear. While inhibitors of lipogenic pathways have been developed as potential therapeutic agents in cancer therapy, their impact on oxidative metabolism is underexplored. Here, we identify the fatty acid synthase (FASN) inhibitor G28UCM as a compound that additionally destabilizes mitochondrial fatty acid synthase (mtFAS) and succinate dehydrogenase subunit B (SDHB), thereby targeting cytosolic and mitochondrial metabolism. Unexpectedly, the decreased abundance of SDHB was linked to disruption of mtFAS, most notably downregulation of Lipoyl Synthase (LIAS). G28UCM induced profound metabolic stress, including pseudohypoxia, oxidative stress, endoplasmic reticulum stress, and ferroptosis. In contrast, genetic depletion of FASN failed to reproduce these effects. In addition to investigating the mechanism of action of G28UCM, our study revealed a genetic interaction between FASN and SDHB, establishing that their dual but not single loss of function is sufficient to impair tumor growth. The synthetic interaction was conserved across prostate cancer, neuroendocrine tumors, and renal carcinoma cell models, including patient-derived cells, and combined inhibition of FASN and SDH markedly suppressed tumor progression in a breast cancer mouse model. Our findings point to new therapeutic opportunities for FASN inhibition beyond tumor initiation, with particular relevance to cancers associated with malignant SDHB mutations.

1. Introduction

Dysregulation of fatty acid (FA) biosynthesis and lipid metabolism contributes to oncogenic signaling and cancer development. *De novo* FA synthesis is driven by fatty acid synthase (FASN), a cytosolic multidomain lipogenic enzyme. FASN catalyzes the condensation of acetyl-CoA and malonyl-CoA to form a β-ketoacyl-acyl carrier protein (ACP) intermediate, which undergoes sequential cycles of condensation, reduction, and dehydration, mediated by distinct FASN subdomains. This process elongates the intermediate to yield the 16-carbon (C)

* Correspondence to: University of Veterinary Medicine Vienna, Austria.
E-mail address: karin.nowikovsky@vetmeduni.ac.at (K. Nowikovsky).
[1] Equal contribution

https://doi.org/10.1016/j.phrs.2026.108087
Received 31 October 2025; Received in revised form 30 December 2025; Accepted 4 January 2026
Available online 9 January 2026

saturated FA palmitate. Through subsequent modifications palmitate can be converted to other FAs involved in the synthesis of cellular membranes and in cellular signaling [1]. Oncogenic signaling frequently upregulates FASN activity, thereby providing membrane lipids required for rapid tumor cell growth, proliferation, and survival. While the expansion of the plasma membrane supports cell division, the expansion of endoplasmic reticulum (ER) membrane helps maintain ER homeostasis during elevated protein synthesis and mitigates ER stress through the unfolded protein response (UPR) [2].

Aside cytosolic FA biosynthesis, mitochondria have retained their ancestral machinery, the mitochondrial fatty acid synthase (mtFAs), to produce their own FAs. mtFAS activity is sequential and begins with the

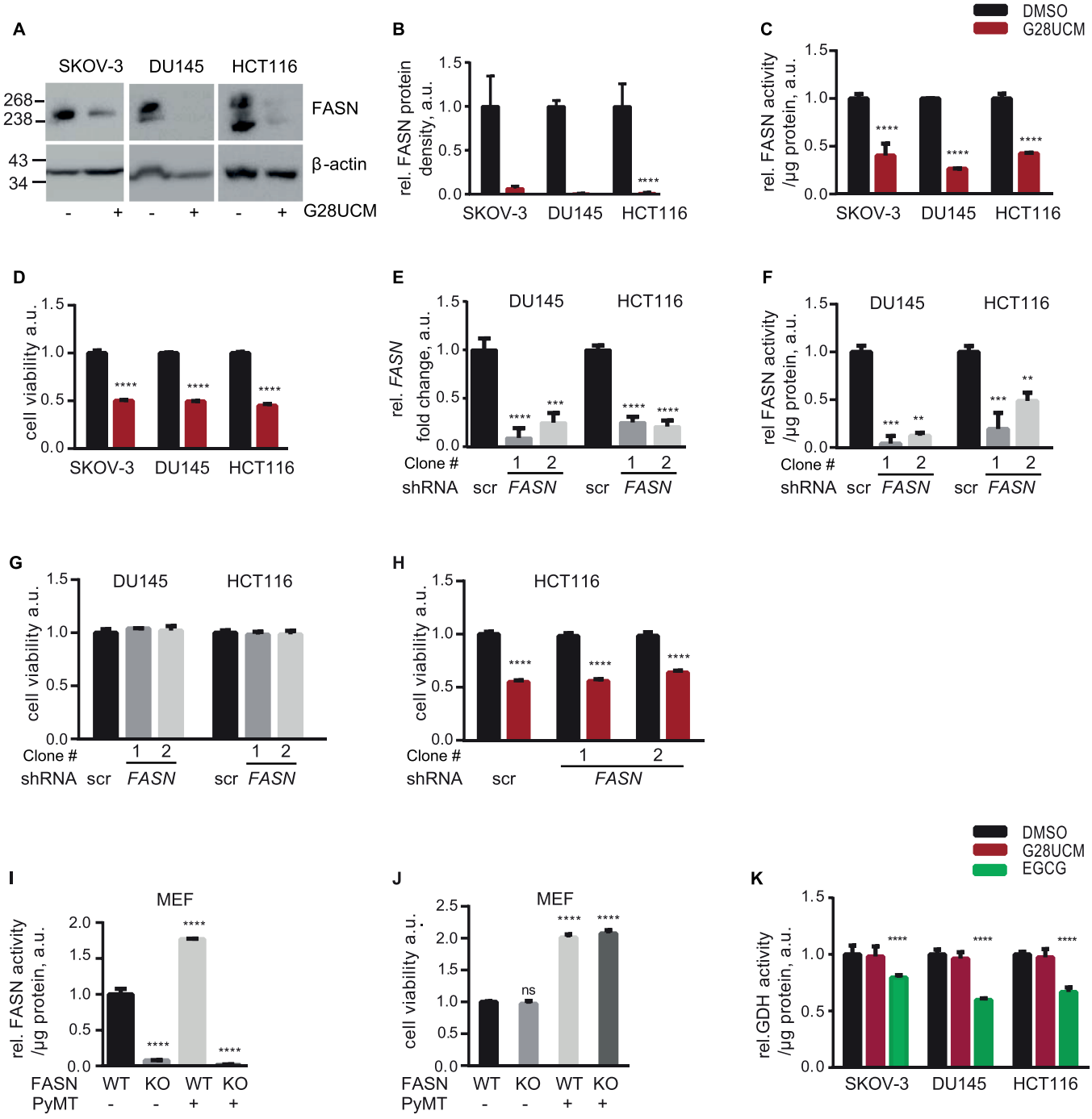

Fig. 1. Drug, but not genetic, inhibition of FASN causes rapid cell death. (A-C) SKOV-3, DU145 and HCT116 cells treated 72 h with G28UCM (red bars) at the respective IC_{50} values (Fig. S1) or vehicle (DMSO, black bars). Shown are FASN protein levels (A-B), enzymatic activity (C), and (D) cell viability. Values of G28UCM-treated cells normalized to DMSO, (B) SKOV-3 and DU145 n = 2, HCT116 n = 3, $p < 0.0001$ by two-tailed *t*-test; (C-D) n = 3, $p < 0.0001$ by two-tailed *t*-test. (E) qRT-PCR of *FASN* in shRNA scrambe (scr, black bars), and independent shRNA*FASN*, namely clone #1: grey bars, clone #2: light grey bars, n = 3: DU145 clone #1 $p < 0.0001$ and clone #2 $p = 0.001$, HCT116 clones #1 and #2 $p < 0.0001$. (F) FASN enzymatic activity in shRNA scr and shRNA *FASN*, n = 3, clone #1 $p < 0.001$ and clone #2 $p < 0.01$. (G) Cell viability of DU145 and HCT116 with shRNA scramble. DU145 $p = 0.3697$ and HCT116 $p = 0.2995$. (H) Cell viability of HCT116 scramble or shRNA *FASN* cell lines exposed to DMSO (black bars) or G28UCM (red bars), n = 3, $p < 0.0001$. FASN activity (I) and cell viability (J) of MEFs expressing $FASN^{lox/lox}$ (WT) or $FASN^{-/-}$ (KO) with or without PyMT, n = 3, normalized to FASN WT, $p < 0.0001$, n.s $p = 0.996$. (K) GDH activity of SKOV-3, DU145 and HCT116 cells treated with DMSO (black), G28UCM (red) or EGCG (150 µM, green), n = 3, normalised to DMSO, $p < 0.0001$.

transfer of malonyl groups to mtACP, followed by cyclic condensation, reduction and dehydration reactions to yield a C8-saturated octanoic acid, the precursor of lipoic acid. These steps are catalyzed by discrete monofunctional mitochondrial enzymes that share amino acid sequence and functional homology with the corresponding catalytic subdomains of the multifunctional cytosolic FASN. In a final step, the octanoyl group is processed to lipoic acid by the lipoyl synthase LIAS, and lipoate is then covalently attached to the E2 subunits of mitochondrial 2-ketoacid dehydrogenases by the lipoyltransferase LIPT1. Lipoylation of these dehydrogenases is a crucial determinant of their activity. Unlike cytosolic synthetized FAs, lipoic acid is not involved in membrane biogenesis but primarily functions as an indispensable cofactor for oxidative metabolism [3].

While the oncogenic role of FASN-catalyzed *de novo* lipogenesis is still under investigation, FASN has been recognized as critical for tumor initiation but most likely dispensable in fully transformed cells [4,5]. Nonetheless, FASN is widely recognized as a cancer marker, as its upregulation in many cancers including lung, breast, colon, prostate, ovarian, and renal cancer is associated with increased proliferation, poor prognosis, and acquired drug resistance, highlighting its potential as an attractive therapeutic target [6–8]. Many FASN inhibitors already confirmed their anticancer and apoptotic activities in tumor cell lines [9–11]. In this study, we employ the epigallocatechin gallate (EGCG) derivative and FASN inhibitor G28UCM [8,12] to dissect the effects of chemical versus genetic inhibition of FASN that were consistent across different cancer models, uncovering an unexpected link between cytosolic and mitochondrial fatty acid synthesis. We identify previously unrecognized FASN-independent mitochondrial off-targets of G28UCM and reveal a novel synthetic metabolic vulnerability that connects lipid metabolism to mitochondrial dysfunction, ultimately impairing tumor growth.

2. Results

2.1. FASN silencing is viable in a number of cancer cell models

Exposure of established ovarian (SKOV-3), prostate (DU145), and colon (HCT116) cancer cell lines to G28UCM (at their respective IC_{50} concentrations, Fig. S1A-B) resulted in reduced FASN protein levels and enzymatic activity (Fig. 1A–C), accompanied by a significant decrease in cell viability (Fig. 1D and Fig. S1C-D). Sensitivity to G28UCM increased proportionally with fetal bovine serum (FBS) reduction, supporting the notion that these cells rely on *de novo* lipid synthesis when FBS-derived lipids become limited (Fig. S1E). To verify the vital role of FASN, we silenced *FASN*. To our surprise, *FASN* knockdown (*FASN KD*), which robustly decreased *FASN* mRNA and enzymatic activity, had no antiproliferative or lethal consequence (Fig. 1E-G and Fig. S1F). Interestingly, G28UCM also remained lethal in absence of FASN (Fig. 1H), raising the possibility of an off-target. To investigate a complete FASN knockout, we next used a tumor model that consisted of a set of mouse embryonic fibroblasts (MEF) derived from mouse $FASN^{lox/lox}$ or $FASN^{-/-}$ with or without overexpression of the oncogene Polyomavirus middle T antigen (PyMT) [5,13]. FASN knockout (KO) did not affect viability in either non-oncogenic or PyMT transformed MEFs (Fig. 1I-J). These results confirmed that FASN loss is tolerated, both in normal and oncogenic contexts.

Because G28UCM is a derivative of EGCG, a natural inhibitor of glutamate dehydrogenase (GDH), essential for tumor growth [14], we investigated whether its unexpected off-target drug toxicity could result from concomitant inhibition of FASN and GDH. In contrast to EGCG, G28UCM failed to inhibit GDH (Fig. 1K).

2.2. G28UCM treatment, but not genetic FASN silencing, stabilizes HIF-1α through succinate accumulation

To determine whether additional pathways targeted by G28UCM contribute to the divergent effects observed between pharmacological inhibition and genetic silencing of *FASN*, we compared the molecular and phenotypic consequences of G28UCM treatment with those of *FASN KD*. G28UCM robustly induced HIF-1α and its downstream transcriptional targets, including REDD1 (Fig. 2A–D), a stress-response factor activated by reactive oxygen species (ROS), ER stress and energy depletion [15,16]. Of note, REDD1 induction upon G28UCM was abrogated when *HIF-1α* was knocked-down (Fig. 2E-F). We also observed that, while HIF-1α gene targets peaked early (6 h), *REDD1* expression continued to increase at 18 h (Fig. S2). As pseudohypoxia markers were consistently increased across all tested lines, we focused in subsequent analyses on selected representative cell lines. In contrast to chemical FASN inhibition, *FASN KD* did not induce HIF-1α or REDD1 except under hypoxia-mimicking conditions ($CoCl_2$) (Fig. 2G-H), demonstrating G28UCM activates HIF-1α through a mechanism independent of FASN inhibition.

HIF-1α protein stability is regulated via hydroxylation by oxygen-sensitive α-ketoglutarate (α-KG)-dependent prolyl hydroxylases (PHDs), which are competitively inhibited by elevated succinate or fumarate [17,18]. Once hydroxylated, HIF-1α is ubiquitylated by von Hippel Lindau (VHL) for proteasomal degradation [19]. To determine whether G28UCM increases HIF-1α by impairing its degradation, we used the proteasome inhibitor MG132, which further increased HIF-1α accumulation (Fig. 2I–J), ruling out defective degradation. We next assessed whether G28UCM affects hydroxylation by quantifying TCA cycle intermediates that regulate this process. Succinate was predominantly elevated (Fig. 2K, M), while fumarate was decreased (Fig. 2L, N). In contrast, *FASN* silencing in DU145 cells or MEFs had no effect on succinate (Fig. 2O–P). However, similar to G28UCM, it led to a modest reduction in citrate and isocitrate levels, and a significant drop in α-KG (Fig. S3A–D).

Collectively, G28UCM, but not *FASN KD*, stabilized and activated HIF-1α, in association with succinate accumulation and cellular stress conditions.

2.3. Drug-induced succinate accumulation results from SDH loss-of-function

Since succinate accumulation and fumarate decrease typically reflect mitochondrial succinate dehydrogenase (SDH) impairment, we evaluated G28UCM's effect on SDH. SDH participates in both the TCA cycle, by oxidizing succinate to fumarate, and the electron transport chain (ETC), by transferring electrons, and can be specifically inhibited by malonate [20]. Similar to malonate, G28UCM inhibited SDH activity (Fig. 3A). In contrast, *FASN KD* or *KO* had no effect on SDH activity, unlike malonate (Fig. 3B–C). Since SDH links the TCA cycle and ETC, we evaluated mitochondrial respiration. G28UCM abolished complex II (CII)-supported respiration (Fig. 3D–E). Complex I (CI)-dependent respiration was also reduced, though to a lesser extent (Fig. 3D–E). Consistently, oxygen consumption rates (OCR) were significantly reduced in G28UCM-treated cells but not in *FASN KD* cells (Fig. S4). To confirm SDH as G28UCM target in a clinical context, we measured enzymatic SDH activity in proliferative ($Ki67^{+}$) *ex vivo* tumor tissue slices from patients, and observed a marked inhibition of SDH activity upon G28UCM treatment (Fig. 3F–G), validating SDH as a G28UCM target in clinical samples.

2.4. G28UCM specifically reduces SDH protein levels and affects mitochondrial lipid synthesis

SDH comprises two catalytic subunits: the flavoprotein SDHA and the iron-sulfur (Fe-S) protein SDHB, whose impairment is sufficient to deactivate the complex. Among these, SDHB was most affected by G28UCM, showing a marked decrease as early as 24 h after drug exposure (Fig. 4A–B). The other respiratory chain subunits, NDUFB8 (CI), UQCRC2 (CIII), and COX2 (CIV), were moderately reduced, while

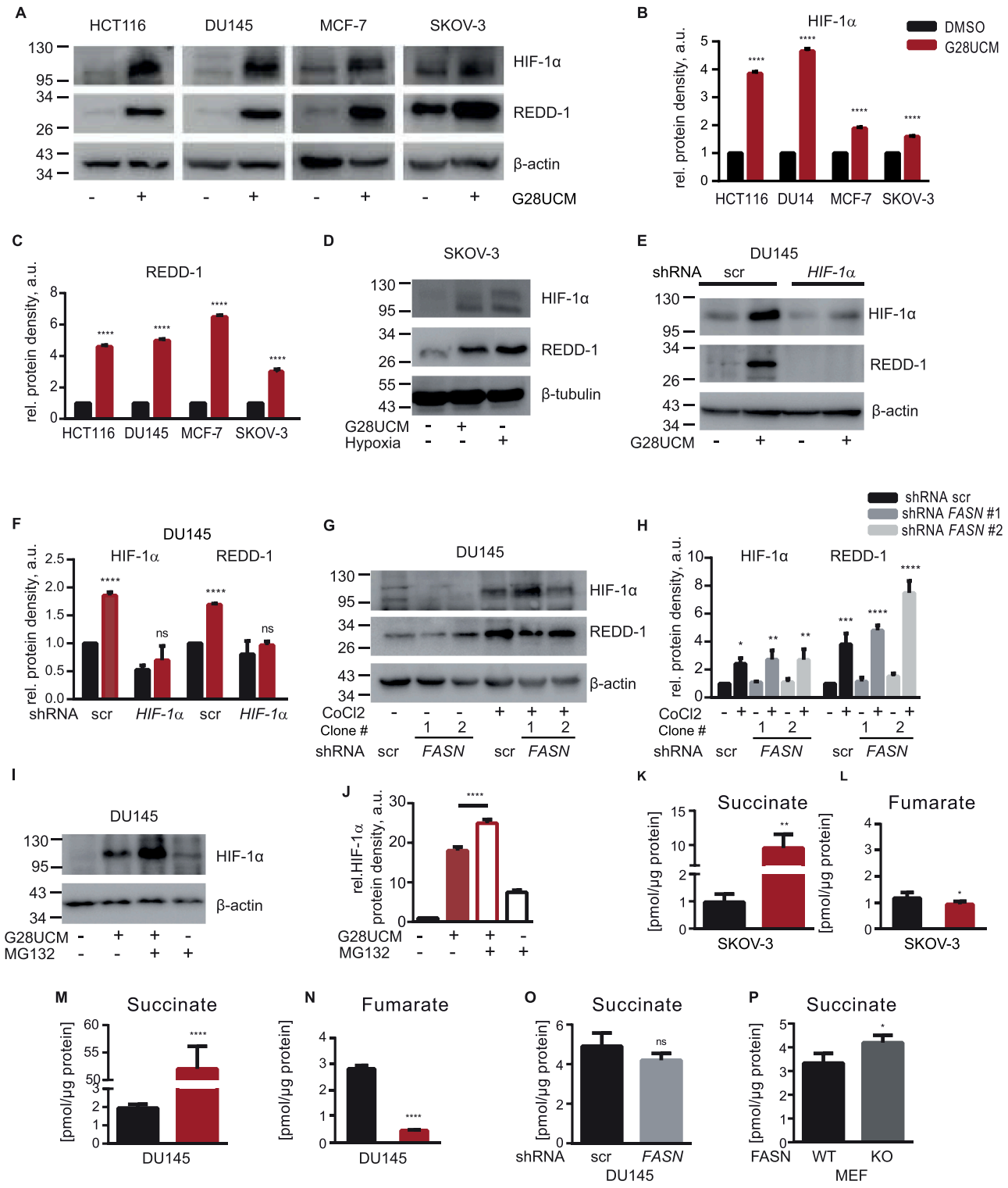

Fig. 2. Drug, but not genetic, inhibition of FASN induces REDD-1 and HIF1-α, and accumulation of succinate. (A) Immunoblots of cells treated with DMSO (-) or G28UCM (+) for 6 hrs and immunoblotted for REDD-1 and HIF-1α and (B-C) densitometry analysis relatively to β-actin n = 3, $p < 0.0001$, two-tailed *t*-test. (D) Immunoblots for HIF-1α and REDD-1 in SKOV-3 cells under control (-), G28UCM or $CoCl_2$- mediated hypoxic conditions (+). (E-F) Immunoblots and quantification of HIF-1α and REDD-1 expression in DU145 scr and *HIF-1α KD* cells exposed to G28UCM (+) or vehicle (-) relatively to vehicle treated scramble control, n = 3 $p < 0.0001$. (G) Immunoblots of HIF-1α and REDD-1 in DU145 *FASN KD* cells (independent shRNA *FASN* clone #1, #2, under control (-) or $CoCl_2$ (+) conditions, (H) densitometry relatively to β-actin, scr control was set as 1, n = 3, *p = 0.1, **p < 0.01, ***p < 0.001,****p<0.0001 one-way ANOVA, Bonferroni's multiple comparison. (I-J) Immunoblots and densitometry of HIF-1α relatively to β-actin under DMSO (black bar) or G28UCM without (red bar) or with (white bar red border) MG132 or MG132 alone (white bar black border), n = 3, $p < 0.0001$ one-way ANOVA, Bonferroni's multiple comparison test. (K-P) Measurement of succinate and fumarate (pmol/µg protein). SKOV-3 (K-L) or DU145 (M-N) treated with vehicle (black bars) or G28UCM (red bars) for 24 hrs; 3 independent experiments (n = 3), each in triplicates and measured by LC-MS. Succinate: SKOV-3 p = 0.0018, DU145 $p < 0.0001$; fumarate: SKOV-3 p = 0.0342, DU145 $p < 0.0001$; two-tailed *t*-test; (O) Succinate: DU145 cells transfected with shRNA scr (black bars) or shRNA *FASN* clone # 1 (grey bars) and (P) MEFs $FASN^{lox/lox}$ (WT) or $FASN^{-/-}$ (KO) over-expressing PyMT. Succinate p = 1.801 and p = 0.0428, respectively, two-tailed t-test.

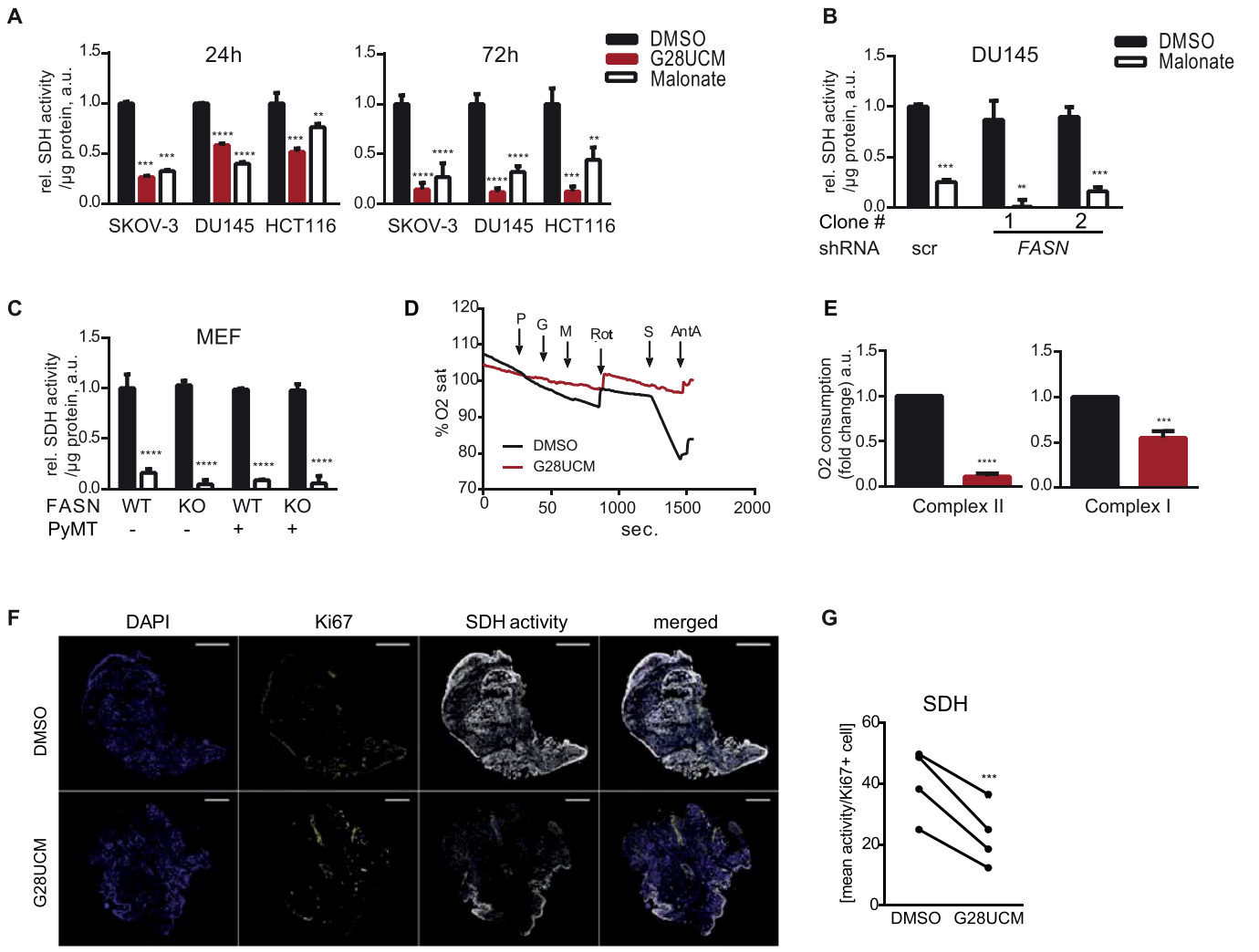

Fig. 3. G28UCM targets SDH and complex II activity. (A) SDH activity of SKOV-3, DU145 or HCT116 cells exposed to G28UCM or vehicle for 24 hrs or 72 hrs or malonate for 15 min. DMSO was set as 1, quantifications n = 3, 24 hrs: SKOV-3 $p < 0.001$ and DU145 $p < 0.0001$, HCT116 $p < 0.0001$; 72 hrs SKOV-3 and DU145 $p < 0.0001$, and HCT116 $p = 0.0003$. (B) SDH activity without or with malonate in DU145 scr set as fold change, and shRNA *FASN* (clones #1 and #2, as indicated), quantification n = 3, scr $p = 0.0009$, clone #1 $p = 0.0017$, clone #2 $p = 0.0003$, one way ANOVA Bonferroni's multiple comparison test. (C) SDH activity in MEFs $FASN^{lox/lox}$ (WT) or $FASN^{-/-}$ (KO) overexpressing or not PyMT without or with malonate. Quantification normalized to $FASN^{lox/lox}$, set as 1, n = 3, $p < 0.0001$. (B-C) one-way ANOVA. (D) Recording of succinate dependent respiration of permeabilized HCT116 cells using a Clark electrode, additions indicated by the arrows: P: pyruvate, G: glutamate, M: malate, Rot: rotenone, S: succinate and AntA: antimycin A (all 10 µM). (E) Quantification of O2 consumption before rotenone $p < 0.001$ and after succinate, $p < 0.0001$, n = 3, two-tailed *t*-test. (F) Representative images of 7 µm thick frozen sections of colon cancer specimens exposed 24 hrs to 50 µM G28UCM or DMSO and stained for the activity of SDH, DAPI and Ki67. Scale bars: 100 µm. (G) Mean SDH-activity ± SEM per Ki67 + cell. Data represents 4 patients each measured in replicates of 2–3, $p < 0.001$ two-tailed paired *t*-test.

ATP5A (CV) remained stable or modestly increased (Fig. 4A–B). In contrast, *FASN KD* or *KO* did not reduce SDHB or any of these units (Fig. 4C–F).

Given the distinct subcellular localization of cytosolic FASN (https://www.proteinatlas.org/ENSG00000169710-FASN) and mitochondrial SDHB, we tested whether G28UCM could impair SDH directly and independently of FASN in isolated mitochondria (Fig. 4G). Immunoblots confirmed the absence of FASN contamination in this fraction. Remarkably, G28UCM inactivated SDH in isolated mitochondria, mirroring the effects of malonate (Fig. 4H), confirming that G28UCM is active in mitochondria and targets SDHB independently of FASN. As a plausible explanation, we hypothesized that G28UCM interferes with the mtFAS pathway, which not only parallels FASN through shared homologies of enzymatic components, but also has a crucial role in controlling SDH assembly [21]. Earlier studies reported a reduced abundance of oxidative phosphorylation (OXPHOS) proteins, most notably SDHB, in cells harboring mutations of the mtFAS beta-ketoacyl synthase OXSM or the terminal reductase MECR [22]. As a first indication in this direction, 48 h of G28UCM exposure decreased OXSM abundance and reduced lipoylation of the E2 subunits of the α-ketoglutarate dehydrogenase (α-KGDH) and pyruvate dehydrogenase (PDH) complexes, DLST and DLAT, respectively (Fig. S5A). To assess earlier changes, as observed for SDHB, we exposed cells to G28UCM for 24 h and detected variably reduced lipoylation of DLST and DLAT in DU145, HCT116, and MEF $FASN^{lox/lox}$ PyMT cells, consistent with a modest decrease in lipoic acid (Fig. S5B-C). Decreased malonyl-CoA-acyl carrier protein transacylase MCAT, and to lesser extent MECR, but not OXSM, was observed in $FASN^{lox/lox}$ PyMT MEF and DU145 cells (Fig. S5B-C), suggesting that OXSM loss represents a later event. In particular, LIAS, a Fe-S cluster–containing enzyme required for the conversion of octanoic acid to lipoic acid and the stability of other Fe-S proteins including SDHB, was consistently downregulated in $FASN^{lox/lox}$ PyMT, DU145, and HCT116 cells (Fig. 5A-B). Because LIAS and SDHB showed the most pronounced alterations, we examined whether these changes were

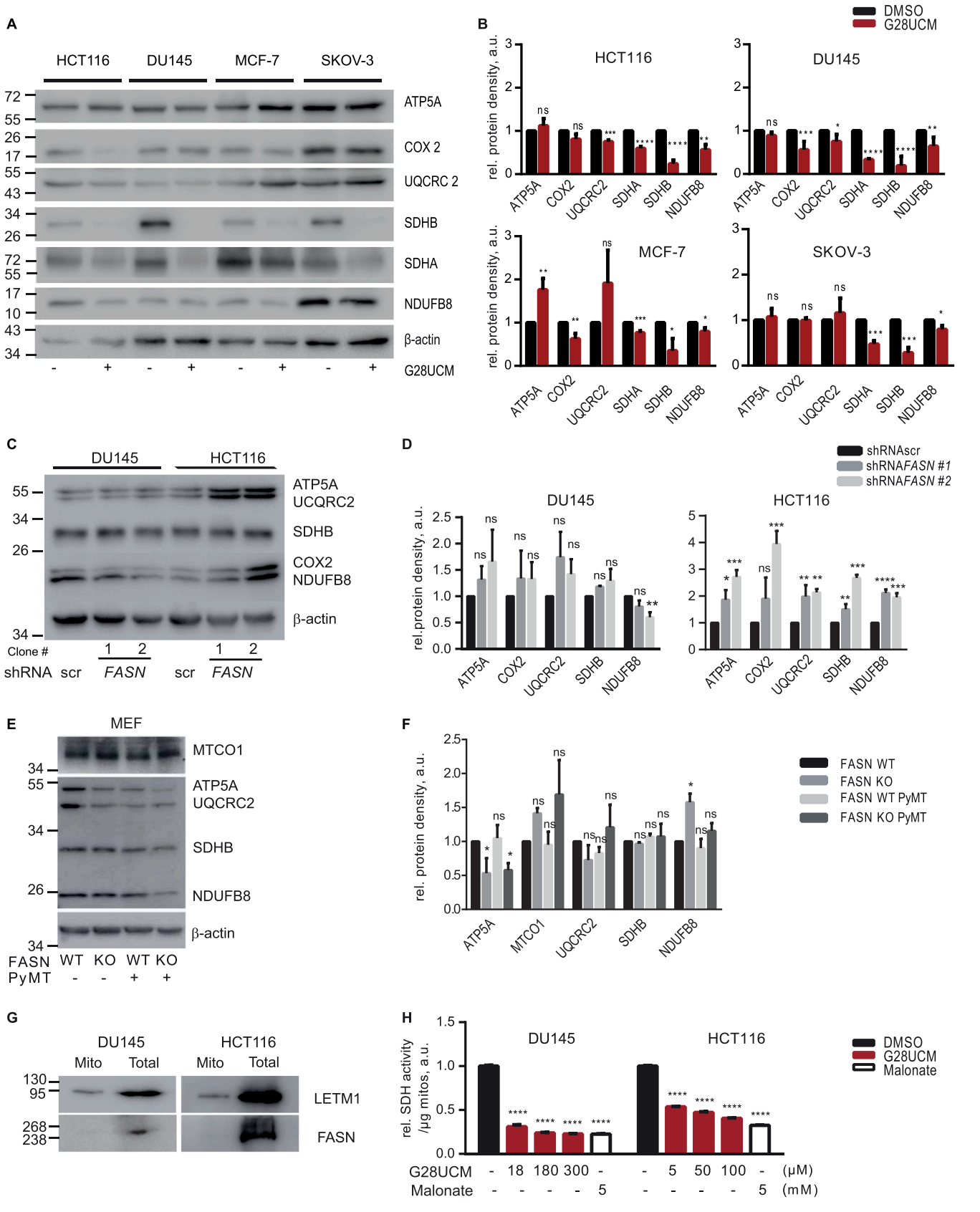

(caption on next page)

Fig. 4. G28UCM specifically targets SDHB among other mitochondrial respiration chain components. (A) Immunoblots of lysates of cells treated 24 hrs with vehicle (DMSO) (-) or G28UCM (+). (B) Densitometry relatively to β-actin, n = 3; HCT116 cells: ATP5A p = 0.2573, COX2 p = 0.0501, UQCRC2 p = 0.0005, SDHA p = 0.0001, SDHB p < 0.0001, NDUFB8 p = 0.0032; DU145 cells: ATP5A p = 0.348, COX2 p = 0.0009, UQCRC2 p = 0.0237, SDHA and SDHB p < 0.0001, NDUFB8 p = 0.0047; MCF-7 cells: ATP5A, p = 0.0070, COX2, p = 0.0064, UQCRC2 p = 0.1069, SDHA p = 0.0007, SDHB p = 0.0165, NDUFB8 p = 0.0153; SKOV-3 cells: ATP5A p = 0.5323, COX2 p = 0.8750, UQCRC2 p = 0.4506, SDHA p = 0.0002, SDHB p = 0.0004, NDUFB8 p = 0.0153,two-tailed *t*-test. (C) Immunoblots of cell lysates from DU145 and HCT116 expressing shRNA scr, shRNA*FASN* #1 or shRNA*FASN* #2 or (E) from MEFs with FASN WT or KO expressing or not PyMT and densitometric analysis, n = 3. (D) DU145: ATP5A in shRNA*FASN* #1 p = 0.5256, shRNAshRNA*FASN* #2 p = 0.12323, COX2 in shRNA*FASN* #1 p = 0.4497, shRNA*FASN* #2 p = 0.4694, SDHB in shRNA*FASN* #1 p = 0.2258, shRNA*FASN* #2 p = 0.0560, UQCRC2 in shRNA*FASN* #1 p = 0.0536, shRNA*FASN* #2 p = 0.2687, NDUFB8 in shRNA*FASN* #1 p = 0.0569, shRNA*FASN* #2 p = 0.0023; HCT116: ATP5 in shRNA*FASN* #1 p = 0.0121, shRNA*FASN* #2 p = 0.0004, COX2 in shRNA*FASN* #1 p = 0.1438, shRNA*FASN* #2 p = 0.0009, SDHB in shRNA*FASN* #1 p = 0.0059, shRNA*FASN* #2 p = 0.0001, UQCRC2 in shRNA*FASN* #1 p = 0,0065, shRNA*FASN* #2 p = 0.0031,NDUFB8 in shRNA*FASN* #1 p = 0.0001, shRNA*FASN* #2 p = 0.001. (F) ATP5A in FASN KO p = 0.0189, FASN WT PyMT p > 0.999, FASN KO p = 0.0321; MTCO1 in FASN KO p = 0.6131, FASN WT pYMT p > 0.999, FASN KO PyMT p = 0.1954; UQCRC2 in FASN WT p = 0.7559 FASN WT PyMT p > 0.999, FASN KO PyMT p > 0.999; SDHB all p > 0.999; NDUFB8 in FASN KO p = 0.0191, FASN WT PyMT p > 0.999, FASN KO PyMT p = 0.7002. (G) Immunoblot of DU145 and HCT116 isolated mitochondrial (Mito) and total fractions. LETM1 served as mitochondrial loading control. (H) SDH activity of mitochondria isolated from DU145 (left) or HCT116 (right) and exposed to DMSO (black bars) or the indicated concentration of G28UCM (red bars) for 45 min or to malonate (white bars) for 15 min. n = 3, quantification relatively to DMSO (set as 1), p < 0.0001 one-way ANOVA.

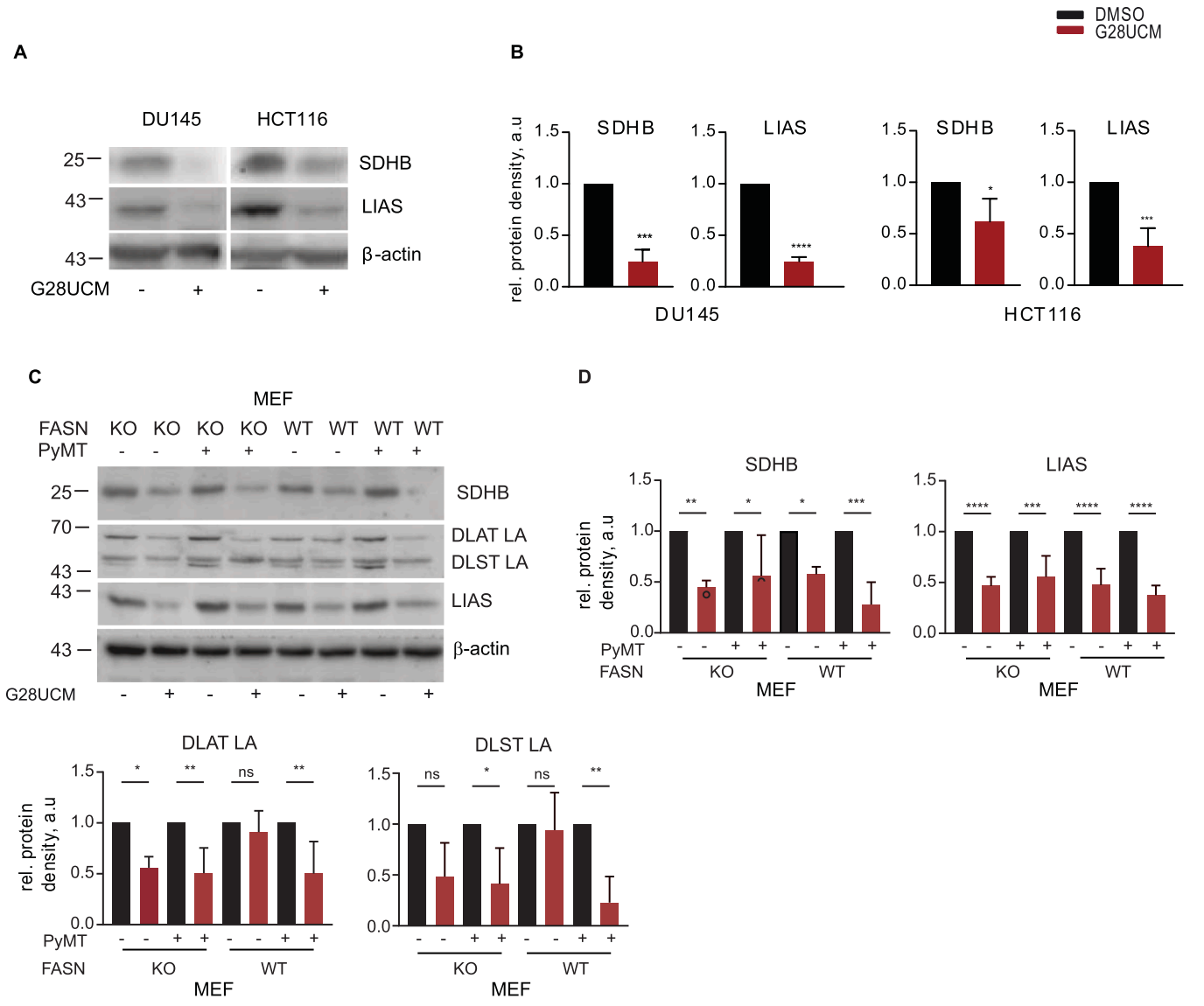

Fig. 5. G28UCM decreases LIAS. Immunoblots of cell lysates from (A) DU145 and HCT116 cells treated 24 hrs with vehicle (-) or G28UCM (+) decorated with indicated antibodies, β-actin serving as loading control, and (B) densitometry analysis relatively to β-actin n = 3, DU154: SDHB p < 0.001, LIAS p < 0.0001, HCT116: SDHB p < 0.5, LIAS p < 0.001, two-tailed Student *t*-test. (C) Immunoblots showing SDHB, DLAT-LA, DLST-LA, and LIAS in MEF FASN KO and FASN WT with and without PyMT, treated with DMSO or G28UCM. Densitometry relatively to β-actin, n = 3, one way ANOVA with Bonferroni correction. SDHB in FASN KO, FASN KO PYMT, FASN WT and FASN WT PyMT p < 0.01, p < 0.5, p < 0.5 and p < 001, respectively, LIAS p < 0001, p < 0.001, p < 0.0001 and p < 0.0001, DLST-LA p = 0.0602, p = 0,0280, p = 0.9967 and p = 0.0037, DLAT-LA p < 0.5, p < 0.01, p = 0–2022, p < 0.01.

dependent on FASN expression and the oncogenic context. G28UCM decreased LIAS and SDHB levels in both PyMT-transformed and non-transformed cells, irrespective of FASN deletion (Fig. 5C-D). These findings indicate that G28UCM impairs LIAS independently of FASN status and oncogenic transformation, thereby disrupting SDH and lipoic acid biosynthesis.

2.5. Oxidative and ER-stress contributes to cell death

While palmitate, the end product of FASN, has been shown to increase G28UCM toxicity [23], lipoic acid significantly protected from G28UCM-induced cell death, as did the unsaturated cytosolic FA oleic acid (Fig. S6A-B), suggesting that both may confer protection through antioxidant mechanisms.

Loss of SDHB leads to disassembly of CII, releasing Fe-S clusters and increasing free intracellular iron. In the context of impaired OXPHOS, this excess iron promotes ROS production via the Fenton reaction [24]. Consistent with this, G28UCM-treated HCT116 and DU145 cells displayed elevated mitochondrial ROS and an even higher accumulation of total intracellular ROS (Fig. 6A–B). To explore an involvement of iron-related stress in ROS formation, cells were pretreated with ferrostatin-1 (Fer1), a lipophilic antioxidant that counteracts lipid peroxidation and ferroptosis. While Fer1 had no significant effect on mitochondrial ROS, it markedly reduced total ROS in both cell lines. These findings suggest that distinct subcellular sources contribute to overall oxidative stress, with iron-dependent lipid peroxidation occurring primarily in non-mitochondrial compartments. As oxidative and ER stress are often linked, we examined ER stress markers of the UPR. G28UCM upregulated BiP, a master regulator of the UPR, and IRE1α, a central ER stress sensor and signaling kinase. Co-treatment with Fer1 significantly blunted the induction of both BiP and IRE1α (Fig. 6C–E), suggesting that oxidative membrane damage promotes ER stress. Mechanistically, BiP activates ATF6, which in turn promotes *XBP1* transcription, while IRE1α catalyzes splicing of *XBP1* mRNA into the stable, active isoform *s-XBP1*, a transcriptional activator of lipogenic genes [25]. G28UCM significantly increased both total *XBP1* and *s-XBP1* mRNA, while Fer1 co-treatment reversed these effects (Fig. 6F), further implicating oxidative stress in UPR activation.

Consistent with structural alterations in the ER, transmission electron microscopy revealed that G28UCM-treated cells exhibited a transition from the typical sharp-edged ER cisternae with narrow lumina to dilated, undulated, and blistered membranes (Fig. 6I–L). Similar membrane blebbing was observed in plasma membranes under mtFAS ablation, which caused OXPHOS deficiency, superoxide accumulation and increased susceptibility to lipid peroxidation [26]. More severely affected regions exhibited pronounced ER deformation and enlarged luminal spaces (Fig. S6), consistent with ER stress. We further assessed the contribution of oxidative stress to G28UCM-induced cytotoxicity. Pretreatment of cells with Fer1 partially restored cell viability (Fig. 6G–H), suggesting that oxidative damage and lipid peroxidation participate in G28UCM-triggered ferroptosis-like cell death.

2.6. Dual, but not single, ablation of SDHB and FASN induces synthetic lethality

Overall, the data suggest that G28UCM has a dual mechanism of action, targeting both FASN and mitochondrial metabolism, including respiration and lipogenesis. Since mtFAS inhibition is detrimental to non-transformed cells [22], and lipoic acid synthesis is essential, as evidenced by the lethality of *MCAT*, *OXSM*, *MECR*, or *LIAS* knockouts [21], we tested whether dual inhibition of FASN and SDH is sufficient to compromise cancer cell viability. We individually or simultaneously silenced *SDHB* and *FASN* in DU145 cells (Fig. 7A–B). Single knockdowns had minimal effects (Fig. 7C), but co-silencing both genes led to a proportional reduction in viability, correlating with silencing efficiency. These results support a synthetic lethal interaction between *SDH* and *FASN*.

2.7. FASN KD induces cell death in neuroblastoma cells with SDHB loss-of-function

Pheochromocytoma (PCC) and paraganglioma (PGL) are rare but malignant neuroendocrine tumors that underlie SDHB loss-of-function (LOF) germline mutations [27]. In absence of established human PCC/PGL cell lines (PGGCs), *SDHB KD* in SK-N-AS cells is a widely accepted neuroblastoma model for these SDHB-deficient tumors [28]. We transiently transfected SK-N-AS cells with shRNAs targeting *SDHB*, *FASN* or both, yielding a knockdown efficiency of approximately 50–60 % (Fig. 7D–E). While individual knockdowns did not affect proliferation, concurrent knockdown of *FASN* and *SDHB* led to a $>$ 50 % decrease in viability (Fig. 7F–G), mirroring the effect observed with G28UCM treatment (Fig. 7H). This result support a synthetic lethal interaction between *FASN* and *SDHB*.

2.8. FASN silencing impairs viability in SDH-mutant renal carcinoma cells

The pathogenic $SDHB^{R46Q}$ mutation, identified in PGGCs and renal cancer cells (RCCs), causes SDH disassembly, succinate accumulation, global hypermethylation and aggressive tumor growth [29]. We used UOK269 renal cancer cells harboring the $SDHB^{R46Q}$ mutation and compared these cells expressing an empty vector (UOK296EV) or a rescue vector with wild-type *SDHB* (UOK269WT) [29].

Treatment with malonate inhibited SDH activity in UOK269WT but had no effect in UOK269EV, confirming the rescue of active SDH in UOK269WT and the inactive SDH in UOK269EV cells (Fig. 7I). *FASN* knockdown was equally efficient in both cell lines (Fig. 7J), but only reduced viability in UOK269EV cells (Fig. 7K). These results demonstrate that FASN suppression selectively affects SDH-deficient cells, consistent with a synthetic lethal interaction.

2.9. Administration of malonate in PyMT FASN KO mice prevents tumor growth

To test the synthetic lethal interaction of FASN and SDHB *in vivo* in the MMTV-PyMT transgenic mice [4], where Polyomavirus middle T (PyMT) oncogene is expressed under the control of the MMTV promoter, leading to the development of ductal breast carcinoma. At 7 weeks of age, approximately 100 % of the animals had invasive ductal carcinomas with features that recapitulate the human luminal B tumors [30]. To genetically ablate FASN, $FASN^{lox/lox}$;Tg UBC-CreERT2 mice were crossed with MMTV-PyMT animals, and systemic Cre activity was induced with tamoxifen, as described in [4], resulting in efficient FASN KO (Fig. 8A-B). To suppress SDH activity, we performed intratumoral injections of dimethyl malonate and the mean tumor burden was compared in the 4 groups after 3 weeks. Malonate effectively reduced SDH activity in both FASN WT and FASN KO background (Fig. 8C). Notably, tumor growth was substantially reduced in the PyMT FASN KO + malonate cohort but not in any single treatment (PyMT FASN KO + vehicle or PyMT FASN WT + malonate) cohort (Fig. 8D). BiP was selectively elevated in the PyMT-FASN-KO + malonate cohort (Fig. 8E). Collectively, these results suggest that concurrent FASN and SDH deficiency triggers ER stress, and confirmed that dual abrogation of FASN and SDHB suppresses tumor growth *in vivo*, consistent with the synthetic lethality identified *in vitro*.

3. Discussion

3.1. Discrepancy between genetic ablation and pharmacological inhibition

Our study uncovers an off-target impact of chemical FASN inhibition on mtFAS and a previously unrecognized connection between LIAS and

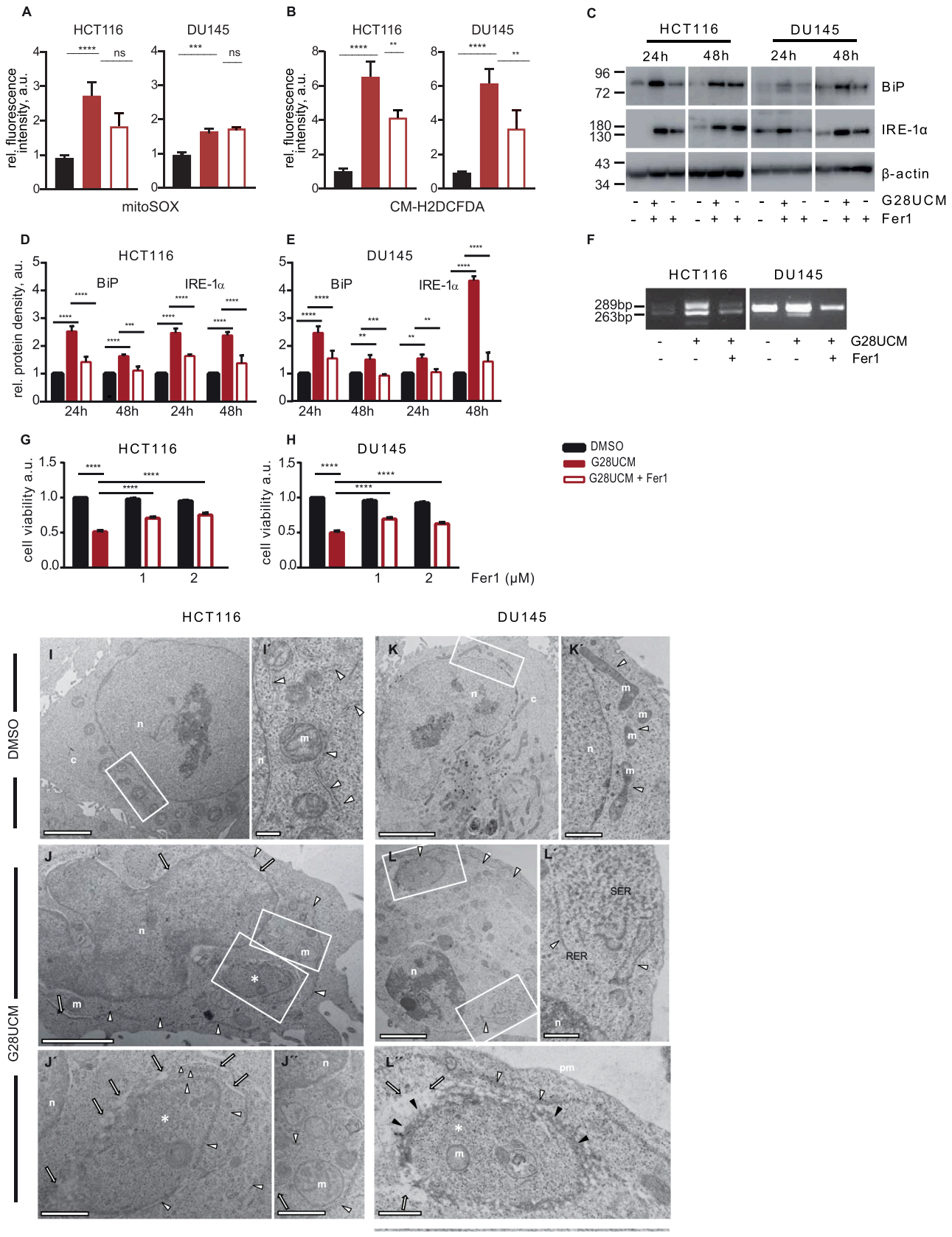

(caption on next page)

Fig. 6. G28UCM induces oxidative and ER stress, which is reverted by Ferostatin1. Indicated cells exposed to DMSO or G28UCM 48 hrs were stained with MitoSOX (A) or CM-H2DCFDA (B) in presence (+) or absence of ferrostatin (Fer1) (2 μM) and the fluorescence changes were quantified from n = 3, statistical analysis: one way ANOVA with Bonferroni correction (ns: $p = 0.8954$, *$p < 0.05$, **$p < 0.01$, ***$p < 0.001$, ****$p < 0.0001$). (C) Immunoblots of the indicated cells treated for 24 or 48 hrs with DMSO or G28UCM with (+) or without (-) Fer1. β-actin served as loading control. (D-E) Densitometry, n = 3, one-way ANOVA: (D) HCT116 BiP and IRE-1a 24 hrs $p < 0.0001$, BiP 48 hrs $p < 0.001$, $p < 0.0001$, IRE-1a 48 hrs $p < 0.0001$, one-way ANOVA; (E) DU145 BiP 24 hrs $p < 0.0001$ IRE-1a 24 hrs $p < 0.01$, BiP 48 hrs $p < 0.001$, $p < 0.01$, IRE-1a 48 hrs $p < 0.0001$.(F) Agarose gel analysis of a semi quantitative PCR showing unspliced *XBP1* and *s-XBP1* after 72 hrs DMSO or G28UCM treatment. Cell viability of HCT116 (G) and DU145 (H) cells treated with DMSO or G28UCM with or without 1 or 2 μM Fer1 for 72 hrs was assessed by trypan blue exclusion assays, n = 3 $p < 0{,}0001$ one-way ANOVA. (I-L') Transmission electron microscopy of HCT116 (I-J') and DU145 cells (K-L') treated with vehicle (I-I' and K-K') or G28UCM (J-L' and L-L') for 24 hrs. The vehicle-treated cells contain ER that is inconspicuous in the overall view (I, K). At higher magnification [(enlarged boxed area in (I) shown separately in (I'), and in (K) shown in (K')] cross sectioned rough ER decorated with ribosomes is displayed (arrowheads). In contrast, G28UCM treated cells possess an expanded rough ER at the cell periphery that can be recognized already at low magnification (arrowheads in J, L). (J' and J") display the boxed area in (J) in more detail both ER forming characteristic loops encircling cytoplasmic content (asterisks) and dilated ER (arrows). Arrowheads point towards ribosomes that decorate the ER. G28UCM-treated DU145 cells contained also prominent non-lammelar smooth ER (boxed area, bottom right in L). The detail in (L') indicates that the SER network is made of blistered membranes in continuity with the rough ER (arrowheads). (L'), detail of the boxed area, top left in (L), displays severe membrane blistering and undulation of ER that is organized in loops (marked with black arrowheads) as well as a large area of dilated ER (arrow) characterized by an expanded electron-lucent lumen. n- nucleus; c- cytoplasm; m- mitochondrion; RER- rough endoplasmic reticulum; SER- smooth endoplasmic reticulum; pm- plasma membrane. Scale bars: I, K = 5 μm, J, L = 2 μm, J', J'', L, L', L'' = 500 nm.

SDH.

Upregulation of FASN in proliferating tumor cells supports membrane biogenesis, oncogenic signaling, and metabolic adaptation, establishing it as hallmark of malignant growth. Although these features make FASN a promising therapeutic target, recent evidence suggests that its crucial role lies primarily in the early stages of cell transformation and tumor initiation rather than in established cancers [5]. Consequently, FASN inhibition may be more effective in prevention than in therapeutic interventions.

Consistent with this view, we found that genetic ablation of FASN was well tolerated across several established models of cancers, whereas treatment with the FASN inhibitor G28UCM was cytotoxic. This divergence indicates that the lethality of pharmacologic perturbation stems from broader metabolic disruption beyond FASN. Such discrepancies between genetic and pharmacological approaches can expose unforeseen metabolic vulnerabilities in cancer cells. Here, we demonstrate that G28UCM treatment destabilizes SDHB, leading to SDH inhibition, succinate accumulation, and HIF-1α activation. Supported by the consistent effects observed across diverse cancer models, cell culture systems, and clinical colon tissue samples, these findings prompted us to investigate the mechanism underlying G28UCM's co-targeting of SDH and to explore the biological significance of its dual activity on FASN and SDHB in complementary model systems.

While a few FASN inhibitors can affect the mitochondrial ETC, largely through repression of β-oxidation due to malonyl-CoA accumulation [31,32], or potentially through reduced *S*-palmitoylation, thereby destabilization ETC proteins like SDHA [33,34], we considered an additional mechanism involving mtFAS. Specifically, based on the homology between FASN and mtFAS enzymes, and previous evidence that loss of key mtFAS catalytic components destabilizes respiratory complexes [22], we hypothesized that mtFAS may be a relevant co-target mediating SDHB destabilization. Indeed, G28UCM reduced protein lipoylation, and LIAS alongside SDHB, hallmarks of mtFAS impairment. Co-targeting mtFAS decreased OXPHOS components beyond CII and impaired oxidative respiration. The marked decline in OCR aligns with prior observations in SDHB and LIAS deficient cells [29,35]. It is also noteworthy that LIAS has been identified as HIF-1α activator through genetic screening. Although complete *LIAS KO* is lethal, rare surviving clones displayed defective lipoylation and α-KGDH inactivation, causing L-2-hydroxy-glutarate (L-2HG) accumulation that stabilizes HIF-1α [35]. Thus, concurrent impairment of LIAS and SDH by G28UCM may synergistically perturb mitochondrial metabolism, and further enhance HIF-1α stabilization.

While it remains unclear whether LIAS is the primary mitochondrial target of G28UCM, it will be important to investigate how LIAS influences SDH stability. Several observations support a role for Fe-S clusters in the interplay between LIAS and SDHB. SDHB is the Fe-S subunit of complex II which is responsible for the electron transfer from succinate oxidation to the ubiquinone pool. LIAS contains two Fe-S clusters, one of them serving as sulfur donor to other proteins, such as SDHB, for their formation of new clusters. SDHB has two leucine-tyrosine-arginine (LYR) motifs that are essential for Fe-S cluster incorporation and SDH assembly. The LYR Fe-S transfer motifs have actually emerged as hotspots for malignant mutations, including the R46Q variant present in UOK269^{R46Q} [29]. Together with the association of SDH deficiency with elevated labile iron [36], these features related to the biogenesis and incorporation of the Fe-S cluster into SDHB suggest a critical link between LIAS, SDHB, ROS, and iron dysregulation in response to G28UCM. As Fe-S clusters are required for lipoic acid synthesis and SDH assembly, LIAS deficiency may destabilize SDHB by impairing Fe-S incorporation. This potential mechanism warrants future investigation.

Collectively, the pharmacological disruption of FASN uncovers a previously unrecognized functional link between LIAS and SDHB underscoring the metabolic cross-talk between lipid synthesis and mitochondrial homeostasis.

3.2. *Involvement of ferroptotic vulnerability*

SDHB is a tumor suppressor gene and both germline and somatic mutations act as oncogenic drivers and poor prognosis markers across multiple tumor types [37–39], including RCC, PGL, and PCC, with potential relevance in other cancers [40]. SDHB-deficient cells accumulate succinate and labile iron, leading to pseudohypoxic signaling, iron overload, redox imbalance, and lipid peroxidation, all converging on increased ferroptotic susceptibility [41]. Notably, SDHB loss fails to activate antioxidant responses mediated by superoxide dismutase or the NRF2 pathway to compensate for ROS formation [36], suggesting that SDH-compromised cells rely on alternative antioxidant mechanisms.

FASN has recently been implicated in ferroptosis resistance. By S-palmitoylating USP5, the deubiquitinase of GPX4, FASN stabilizes USP5 and thus prevents the degradation of GPX4, which is a key suppressor of lipid peroxidation and ferroptosis [34]. Beyond S-palmitoylation, FASN may also support cellular redox homeostasis and expand membrane capacity by providing fatty acids and reducing equivalents that maintain ER integrity and buffer oxidative stress. Supplementation with the palmitate derivative oleic acid produced cytoprotective effects. Similar effects were observed with mitochondrial synthetized lipoic acid. Since oleic acid primarily incorporates into ER membranes and reduces susceptibility to ferroptosis [42] and lipoic acid, although it does not restore protein lipoylation, mitigates oxidative stress [26], their cytoprotection likely reflect their antioxidant activity. Conversely, FASN inhibition, as also observed under G28UCM exposure [23,43], leads to accumulation of polyunsaturated lipids, which are highly susceptible to peroxidation and act as potent inducers of ferroptosis [44]. Under conditions of FASN inhibition and mtFAS impairment, the limited

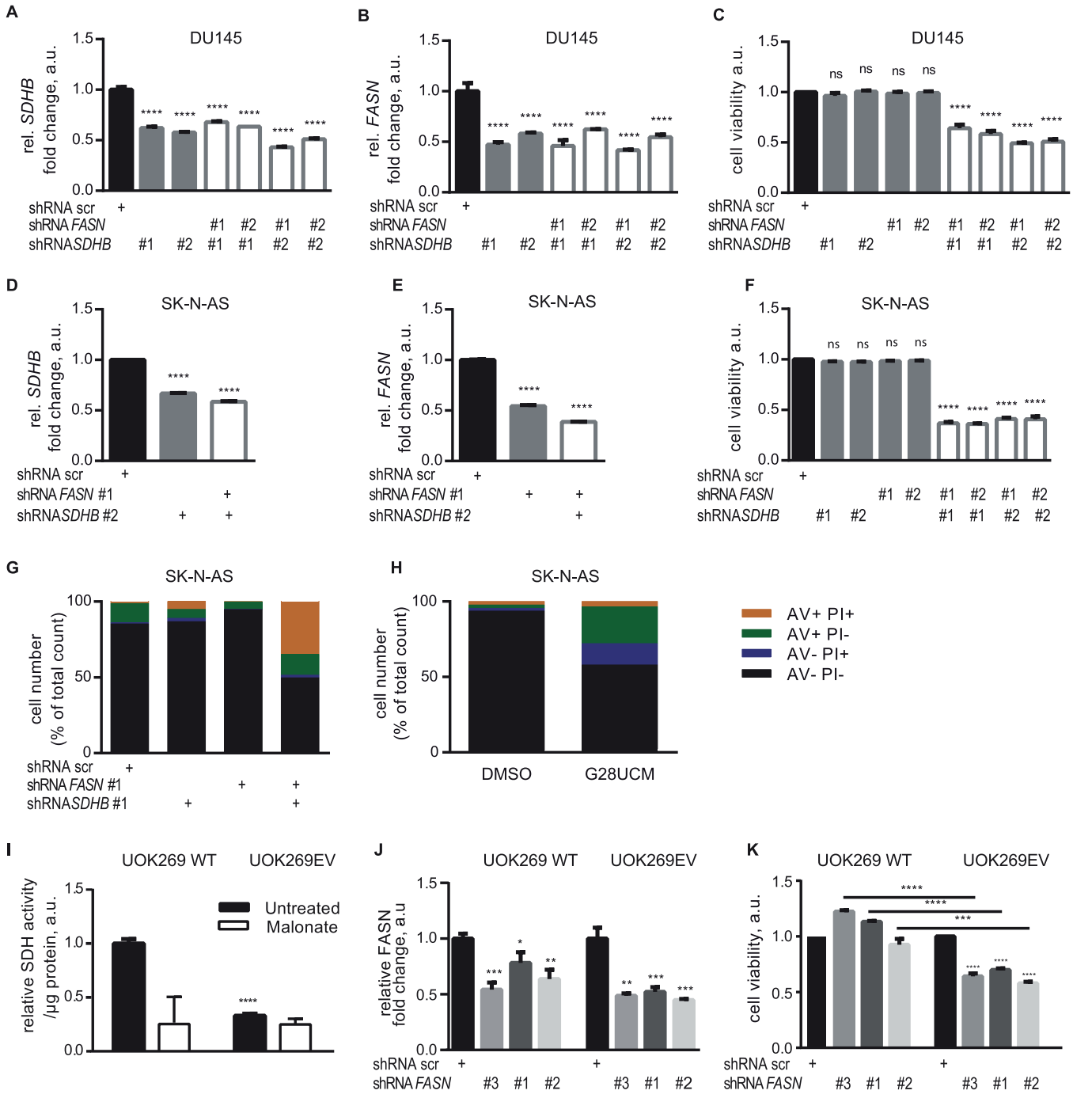

Fig. 7. Synthetic interaction of *SDHB* and *FASN* in cancer models. *SDHB and FASN double knockdown is lethal in DU145 and SK-N-AS.* (A-C) DU145 cells transiently transfected with shRNA scramble (scr), or shRNA *FASN* clone #1 or #2, or shRNA*SDHB* clone #1 or #2, or co-transfected with shRNA*SDHB #1* and shRNA*FASN #1* or *#2* or with shRNA*SDHB #2* and shRNA *FASN #1* or *#2*. (D-G) SK-NA-S cells were transiently transfected with shRNA scramble (scr), or shRNA*SDHB #2* or shRNA*SDHB #2* and shRNA*FASN #1* (D); or with scr or shRNA*FASN #1 or* shRNA*FASN #1* and shRNA*SDHB* #2 (E); or with shRNAscr or shRNA*FASN* #1 or #2 or shRNA*SDHB* #1 or #2, or co-transfected with shRNA*SDHB #1* and shRNA*FASN #1* or *#2* or with shRNA*SDHB #2* and shRNA*FASN #1* or *#2* (F), and after 72 hrs cell death was assessed by trypan blue exclusion assay (C and F) and qRT-PCR performed for the quantification of *SDHB* (A, D) and *FASN* (B, E) gene expression. Cell viability assays n = 3 and qRT-PCR experiments n = 3, $p < 0.0001$, one-way ANOVA, Bonferroniś multiple comparison. SK-NA-S were transiently transfected with scr, or shRNA*FASN #1*, or shRNA*SDHB #1*, or co-transfected with shRNA*FASN #1* and shRNA*SDHB #1* (G) or remained untransfected but treated with DMSO or 43 µM G28UCM for 72 hrs (H) and stained for AV/PI and analyzed by flow cytometry (G-H). *FASN knockdown is lethal in RCC patient's cells with SDHB LOF mutation.* (I) SDH activity with or without malonate in untreated UOK269WT (WT) and UOK269EV (EV) cells. n = 3, EV vs WT $p < 0.0001$, two tailed *t*-test. (J) *FASN* gene expression by qRT-PCR in WT and EV cells transiently transfected with shRNAscr or shRNA*FASN clone #3, #1* or *#2* (n = 3), UOK269WT shRNA*FASN #3* $p = 0.0005$, shRNA*FASN #1* $p = 0.023$, shRNA*FASN #2* $p = 0.0026$, UOK269EV shRNA*FASN #3* $p = 0.0015$, shRNA*FASN #1* $p = 0.0009$, shRNA*FASN #2* $p = 0.0006$ one way ANOVA. (K) Cell viability was assessed by trypan blue exclusion. Viability values of all tested cell lines were normalized to UOK269WT scr which was set as 1. n = 3 UOK269EV shRNA*FASN #3, #1* and *#2* versus UOK269WT, respectively shRNA*FASN #3, #1* $p < 0.0001$, *#2* $p = 0.0004$, two-tailed *t*-test.

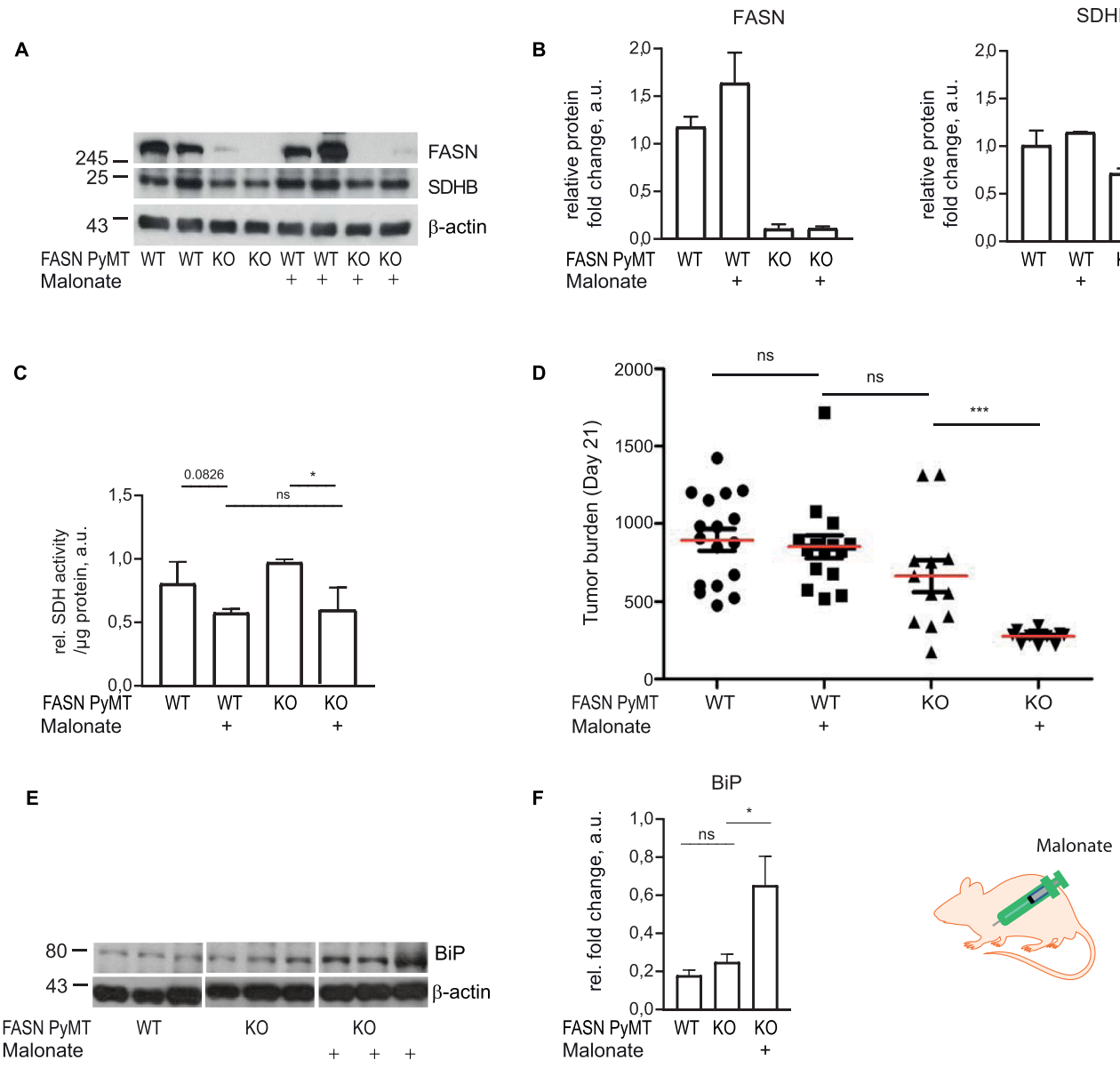

Fig. 8. Malonate reduces SDH activity, upregulates BiP, and delays tumor growth in FASN KO cohorts expressing PyMT. (A) Immunoblot detection of FASN and SDHB levels in FASN KO and FASN WT breast expressing PyMT and treated with vehicle or dimethyl malonate. β-actin served as loading control. (B) Quantification relative to β-actin, n = 2. FASN was depleted, while SDHB remained stable, consistent with malonate's role as a competitive succinate analog that inhibits SDH activity without lowering SDHB levels. (C) Graphs show the mean values ± SEM of SDH activity in the indicated cohorts, n = 3, two-tailed Student *t*-test. FASN KO PyMT treated vs untreated $p < 0.05$ student *t*-test. (D) Tumor size was significantly smaller in PyMT-FASN KO mice treated with dimethyl malonate compared with untreated PyMT-FASN KO mice. After 3 weeks treatment, tumor size was not statistically different in PyMT-FASN$^{lox/lox}$ (WT) mice treated compared with untreated PyMT-FASN WT mice ($p = 0.919$, two-tailed *t*-test) or untreated PyMT-FASN$^{-/-}$ (KO) mice ($p = 0.181$, two-tailed *t*-test). FASN deletion (tamoxifen diet) and SDH inhibition (dimethyl malonate treatment) were induced when the tumors reached 500 mm3 size (day 0). Tumor burden was calculated as tumor volumen (mm^3) at day 21. Scatter plot shows tumor burden in individual tumor for all groups (n = 12–18 tumors per group). (E) Immunoblot detection of BiP and quantification relative to β-actin, ± SEM $p < 0.05$ Student's t test.

availability of lipid-based antioxidant defenses and loss of ER integrity may sensitize cells to ferroptotic death. In line with this, treatment with the lipid radical scavenger Fer1 mitigated ROS accumulation and ER stress, and cell death, supporting a model in which ferroptosis contributes to G28UCM-induced cytotoxicity.

3.3. *Identification of a synthetic lethal interaction between FASN and SDHB*

Because of G28UCM's ability to induce complex metabolic disruptions culminating in cell death and its severe toxicity observed *in vivo* [4], we investigated whether combined genetic perturbation of oncogene *FASN* and tumor suppressor gene *SDHB* could be sufficient to reproduce tumor cell death. While single knockdown of either gene had minimal effect, their combined depletion markedly reduced viability, phenocopying G28UCM. This genetic interaction underscores a conditional dependency of cancer cells on FASN under SDH dysfunction.

Recapitulation of this synthetic interaction in a breast cancer mouse model highlights an unanticipated vulnerability that extends beyond tumor initiation, positioning FASN not only as a target for cancer prevention but also as a therapeutic entry point in SDH-deficient tumors.

A limitation to the generalizability of the study is that, despite the use of a range of *in vivo* and *in vitro* model systems, sex- and gender-related variables were not considered. Future studies will be required

to determine whether sex-dependent differences influence the metabolic and ferroptotic responses identified here.

In summary, our study reveals a metabolic link between cytosolic and mitochondrial fatty acid metabolism in response to G28UCM treatment, connecting lipid synthesis to ferroptosis sensitivity. Although chemical FASN inhibition can trigger unintended and harmful off-target effects, such as loss of LIAS, it also provides mechanistic insight that can guide the design of safer therapies. Notably, dual inhibition of FASN and SDH emerges as a synthetic lethal strategy that exploits cancer-specific metabolic and redox vulnerabilities. The finding that FASN becomes essential under conditions of SDH dysfunction uncovers a hidden metabolic dependency that may help developing targeted therapies for cancers associated with SDH deficiency.

4. Methods

4.1. Cell lines and culture

SKOV-3 cells [23] were cultured in α-MEM (Gibco), HCT116 [45] in McCoy (Sigma), MEFs [4], MCF-7 (ATCC HTB-22), SK-N- AS (ATCC HTB-77) and UOK269 [29] in DMEM (Gibco), DU145 (ATCC HTB-81) in RPMI-164 (Gibco). Culture media were supplemented with antibiotics and 10 % FBS (Gibco), or 5 % FBS during drug treatment. The cell lines were screened for Mycoplasma every 5 months (MycoAlert Lonza kit).

4.2. Reagents

G28UCM was synthesized in high purity as described in [8,46] and solved in dimethyl sulfoxide (DMSO). IC_{50} values in μM: SKOV-3: 43.8, DU145: 18.8, HCT116: 4.71, MCF7: 12.4 (Fig S1A).

A detailed list of reagents is provided in the supplementary information.

4.3. Generation of FASN and SDHB KD

Lipofectamin LTX was used for transfections and puromycin (HCT116 and DU145: 2 μg/mL, SKOV-3 3 μg/mL) for selection. shRNA plasmids against *FASN*: clone #1:TRCN0000003126, clone #2: TRCN0000003127 and clone #3: TRCN0000003128 (Sigma), against *SDHB* 1: clone #1: TRCN0000028083, clone #2: TRCN0000236397 (Sigma), against *HIF-1α*: TRCN0000003810 (Open Biosystems), and scramble: TR20013 (Origene). Single transfections were performed with 1 μg/mL DNA, double transfections with each 0.5 μg/mL DNA. Generation of $FASN^{lox/lox}$ MEFs and subsequent deletion of FASN are described in [4].

4.4. Animal experiments

PyMT+ ; Cre+ $FASN^{-/-}$ and PyMT+ ; Cre+ ; $FASN^{lox/lox}$ female mice [4] were fed with tamoxifen diet (FASN deletion) when the tumors reached 500 mm^3. Dimethyl malonate was dissolved in PBS (pH = 7.4) and administered by intratumoral injection (150 μL volume) at the dose of 10 mM, 3 days per week. Tumor growth was monitored weekly by using calipers. Tumor volumes were calculated using the formula V= (D x d2)/2 mm^3, where D is the largest diameter and d is the shortest diameter. Mice were euthanized in a CO_2 chamber when reaching humane end point (1500 mm^3).

4.5. FASN activity

The FASN activity was determined as described in [47]. Briefly, cells pellets were stored at −80 °C until use, then resuspended in 100 μL FASN activity lysis buffer (1 mM EDTA, 150 mM NaCl, 100 μg/mL PMSF, and 50 mM Tris-HCl, pH 7.5), vortexed and sonicated on ice for 12 min. Cell lysates were centrifuged at 14,000 g for 15 min at 4 °C, and soluble proteins were collected. A total of 96 μg protein was resuspended in 200 μL of 200 mM potassium phosphate buffer (pH 6.6) containing 1 mM DTT, 1 mM EDTA, 240 μM NADPH, and 30 μM acetyl-CoA. Absorbance at 340 nm was recorded for 3 min to determine the background. Malonyl-CoA (50 μM) was then added, samples were incubated 15 min on ice in the dark, and absorbance at 340 nm was measured for additional 3 min. FASN activity was calculated as the difference between the background and the reaction measurements.

4.6. GDH activity

GDH activity was measured using the tetrazolium salt method [48], except that nitroblue tetrazolium was replaced by thiazolylblue and the absorbance wavelength adjusted accordingly for recording at RT using the plate reader (Varioskan Flash, Thermo Scientific).

4.7. Complex II (CII) respiration

Cell pellets were resuspended in KHEB buffer (120 mM KCl, 1 mM EGTA, 5 mM KH_2PO_4, 3 mM HEPES, 0.2 % (w/v) BSA), loaded on each chamber of a Clark electrode (Rank Brothers) and permeabilized with 0.01 % digitonin for 5 min. Basal O_2 consumption was recorded as the decrease in % O_2 saturation.

4.8. SDH activity

SDH activity was assessed using the decylubiquinone-mediated DCPIP reduction (SQR) and PMS-mediated reduction of MTT, as described in [49]. Briefly, cell pellets were kept at −80°C until analysis. Cell permeabilization was verified with trypan blue and sample were subjected to one more freeze-thaw cycle. A total of 96 μg protein were resuspended in 200 μl assay buffer. SQR assay buffer contained 30 mM KH_2PO_4, 20 mM succinate, 2 mM EDTA, and 1 mg/mL BSA pH 7.4) with antimycin A (4 μM), rotenone (2 μM) and 2,6-DCPIP (0.13 mM). Baseline absorbance at 600 nm was recorded at 30 °C for 2 min (plate reader Varioskan Flash, Thermo Scientific) followed by addition of decylubiquinone (0.066 mM) to initiate the reaction, and absorbance was recorded for an additional 4 min. To exclude non-specific activity, malonate (10 mM) was added and absorbance was recorded for further 3 min. CII activity was determined as the change in absorbance upon decylubiquinone addition, corrected for baseline absorbance and non-specific signal after malonate inhibition. For PMS-mediated SDH activity, the assay buffer contained 100 mM Tris-HCl (pH 7.5), 0.5 mM EDTA and 10 mM NaN_3, serving alone or with succinate (20 mM) in the absence or presence of malonate (5 mM). Reactions were initiated by addition of PMS (400 μM) and MTT (150 μM), and absorbance was recorded at 570 nm at 30 °C for 20 min. SDH activity was determined as the succinate-dependent, malonate-sensitive rate of MTT reduction.

4.9. Metabolic imaging of SDH activity in patient tissue samples

Freshly resected colon tumor tissue obtained from four patients diagnosed with primary rectal cancer (AKH, Austria) was evaluated by a pathologist, before releasing for research purposes. Tumor samples were washed in PBS and antibiotica/antifungal cocktail (50 μg/mL gentamycin 1 % pens/strep) cut into blocks of 0.7 mm× 0.7 mm, washed again, and maintained in culture for 24 h at 5 % CO2 and 37 °C in serum free CMRL-HamsF12 (Gibco) medium supplemented with 2 g/L sodiumbicarbonat (Sigma Aldrich) 12 mM glucose and 2 mM GlutaMAX (Gibco) and antibiotic cocktail. After 2 h, matched samples in biological replicates were treated with 50 μM G28UCM or vehicle (DMSO) for 24 hrs with shaking steps to ensure nutrient exchange. Treated samples were embedded in O.C.T. (Tissue-Tek®. Sakura), snap frozen and stored at −80°C. SDH activity was measured on cryosections applying a previously established enzyme-histochemistry protocol [50] and single cell enzyme activities were assessed as previously described [51]. In brief, the tissue sections were defrosted for 5 min and incubated in 0.1 M

Tris-malate buffer pH 8.0 with 10 % polyvinyl alcohol containing 60 mM sodium succinate, 5 mM sodium azide, 5 mM nitroblue tetrazolium chloride and 0.2 mM phenanzine methosulfate. The reaction was stopped after 15 min by washing in warm PBS. After blocking 15 min with blocking buffer (3 % BSA, 5 % FBS and 0.25 % fish gelatin), the tissue was stained for 1 h with an anti-Ki67 antibody (1:50; FITC labelled, BD Bioscience # 612472) followed by 5 min staining with DAPI at room temperature in the dark. After washing the slides with PBS-Tween (0.01 %) and 2 times washing with PBS, the tissue sections were mounted in Fluoroprep (Biomerieux). Acquisition and analysis were performed on a Tissue FAXS histocytometry platform and the raw data, containing all relative intensities for each event (cell), were exported to Excel. The respective mean enzyme activities are defined as relative formazan intensities formed per 15 min per cell. Control reactions were performed in the presence of 250 mM malonic acid and were used for background subtraction.

4.10. Trypan blue exclusion test

0.4 % trypan blue was used with PBS. For each 6 well plate, 3 aliquots (total 900 cells/samples) were counted on a haemocytometer under a transmission microscope.

4.11. Flow cytometric evaluation of ROS

Mitochondrial or total intracellular superoxide levels were assessed by the use of MitoSOX (3 μM) or CM-H_2DCFDA (2 μM), respectively, using CytoFLEX S (Beckman Coulter). The data were analyzed with the with CytExpert 2.4 software.

4.12. Isolation of Mitochondria

Mitochondria were isolated according to [52].

4.13. SDS PAGE and Western blotting analysis

SDS-PAGE and Western blotting analysis were performed in [45]. Antibodies are listed in supplementary information.

4.14. qRT-PCR

Total RNA was extracted using TRIzol reagent and reverse transcribed to cDNA according to [45]. S18 served as reference gene for normalization. Primers were:

S18 fwd: 5′-GTAACCCGTTGAACCCCA-3′, rev: 5′-CCATCCAATCGGTAGTAGCG-3′

SDHB fwd: 5´- TGACTCTACTTTGACCTTCC-3´, rev: 5´-CTTCCTGAGATTCATCCTTC-3´

FASN fwd: 5´-TCGTGCGCTACAGCATGG-3´, rev: 5´-GCCCTCTGAAGTCGAAGA-3´

4.15. Metabolite measurement

Fully $U^{13}C$ labeled yeast extract of *Pichia pastoris* was reconstituted in LC-MS grade water and used as internal standard for LC-MS/MS measurements. All standards were weighed and dissolved in LC-MS grade water. From those stock solutions, different standard calibration levels between 0.01 and 50 μM were prepared in LC-MS grade water with the same aliquot of internal standard in each level.

4.15.1. Sample preparation

For metabolite extraction, an existing protocol for adherent cells (“direct solvent scraping”) was adapted [53]. The following steps were performed on ice. The medium was removed and the cells were washed three times with 1 mL of a PBS solution (4°C). After addition of 50 μL ^{13}C labeled internal standard per well, the cells were scraped in 500 μL ice-cold methanol (80 % v/v in water). The extract was transferred to a sample tube and the wells were washed two times with ice-cold methanol to reach a final volume of 2 mL extract. After centrifugation (15 000 g, 5 min, 4°C), 400 μL aliquots of the cell extracts were dried under reduced pressure. The pellet was used for the determination of the protein content using a 2-D Quant Kit (GE Healthcare). Prior to LC-MS/MS analysis, the dried cell extracts were reconstituted in 100 μL LC-MS grade water.

4.15.2. LC-MS/MS analysis of metabolites

The analysis of metabolites was performed on an LC-MS/MS system. An Agilent 1290 Infinity HPLC system was coupled to an Agilent 6490 triple quadrupole mass spectrometer. Reversed phase separation was performed on an Acquity HSS T3 column (2.1 ×150 mm, 1.8 μm particle size, Waters) operated at a flow rate of 0.25 mL min^{-1}. The column temperature was 40°C and the injection volume 5 μL. Mobile phase A was 0.1 % formic acid in water and B was 100 % methanol. Separation of citric acid, isocitric acid, α-ketoglutaric acid, succinic acid, and fumaric acid was achieved with gradient elution starting with 0 % B for 1 min. In the next 4 min, a linear gradient to 40 % B was applied, followed by 100 % B for 2 min and re-equilibration at 0 % B for 5 min. This resulted in a total run time of 12 min. Mass spectrometric data acquisition was performed in multiple reaction monitoring (MRM) with electrospray ionization (130°C gas temperature, 14 L min^{-1} gas flow, 40 psi nebulizer pressure, 360°C sheath gas temperature, 12 L min^{-1} sheath gas flow, 3000 V capillary voltage) in negative mode. MRM transitions were determined by MassHunter Optimizer software (Agilent Technologies). Precursor masses, product masses for quantifier and qualifier ions, and their specific collision energies are given in Table 1. Data analysis was performed in Agilent MassHunter Quantitative Analysis software. Calibration curves were created using compound specific internal standards based on the peak area ratios of each metabolite and its $U^{13}C$ analog to yield absolute concentrations.

4.16. Study approval

Informed consent was obtained and patient samples were kept anonymously. Clinical tissue samples were procured in alignment with WHO Guiding Principles on Human Cell, Tissue and Organ Transplantation. All tests were performed in accordance with the Declaration of Helsinki good clinical practice guidelines and approval by the Medical University of Vienna Ethics Committee (1651/2013). Animal experiments were approved by the Instituto de Salud Carlos III Ethics Committee (PROEX 387/15) and performed in accordance with the guidelines stated in the International Guiding Principles for Biomedical Research Involving Animals developed by the Council for International Organizations of Medical Sciences and in compliance with the Animal Research: Reporting of In Vivo Experiments (ARRIVE) guidelines for transparent and reproducible reporting.

Table 1
Precursor ions, product ions used as quantifier and qualifier, and collision energies (CE) of the LC-MS/MS analysis.

Metabolite	Precursor ion (*m/z*)	Quantifier		Qualifier	
		Product ion (*m/z*)	CE (V)	Product ion (*m/z*)	CE (V)
Citric acid	191	111	12	87	20
U13C Citric acid	197	116	12	90	20
Isocitric acid	191	111	12	73	20
U13C Isocitric acid	197	116	12	90	20
α-ketoglutaric acid	145	101	4	57	8
U13C α-ketoglutaric acid	150	105	4	60	8
Succinic acid	117	73	8	99	5
U13C Succinic acid	121	76	8	103	5

4.17. Statistics

Data analysis and statistical tests were performed using GraphPad Prism 6 and Microsoft Excel

software. n = independent biological replicates. All quantitative data are as mean ± SD unless other indicated. Two-tailed Student's *t*-test or one-way ANOVA followed by Bonferroni comparison tests, as specified in the figure legends.

CRediT authorship contribution statement

Karin Nowikovsky: Writing – original draft, Visualization, Validation, Supervision, Project administration, Methodology, Funding acquisition, Data curation, Conceptualization. **Nastasia Wilfinger-Lutz:** Writing – review & editing, Visualization, Validation, Methodology, Investigation, Funding acquisition, Formal analysis. **Michaela Schwaiger-Haber:** Writing – original draft, Visualization, Validation, Investigation, Conceptualization. **Wen-An Wang:** Visualization, Validation, Methodology, Formal analysis. **Kristina M. Kuehrer:** Writing – review & editing, Validation, Methodology, Funding acquisition, Formal analysis. **Maria J. Bueno:** Writing – review & editing, Visualization, Validation, Methodology, Conceptualization. **Miguel Quintela-Fandino:** Supervision, Methodology, Conceptualization. **Arvand Haschemi:** Supervision, Methodology. **Gunda Koellensperger:** Supervision, Methodology. **Ronald Mekis:** Visualization, Validation, Investigation, Formal analysis. **Anne Miller:** Methodology, Data curation. **Katrin Krejci:** Visualization, Methodology, Investigation, Formal analysis. **Nicolle Gobbo Oliveira Erünlü:** Visualization, Investigation. **Michael Bergmann:** Resources. **Oscar Yanes:** Methodology, Data curation. **Alexandra Junza:** Investigation. **Siegfried Reipert:** Writing – original draft, Visualization, Validation, Investigation, Data curation.

Declaration of Competing Interest

All authors also declare that they have no conflict of interest.

Acknowledgements

We thank Prof M. Linehan (NIH, National Cancer Institute, Bethesda) for providing UOK269EV and UOK269WT cells, M. L. López-Rodríguez and JR Garcia-Carceles (Complutense University of Madrid) and R. Colomer (CNIO, Madrid) for synthetizing and providing G28UCM, M. Billerhart for preliminary tasks, L. Wimmer for expert technical assistance, T. Grunt for fruitful discussion, S. Nowinski, E. Tomasich, Dr. D. Abraham, S. Trojanek, P. Volejnik, M. Hilgarth, and the Core Facility Cell Imaging and Ultrastructure Research of the University of Vienna for technical support. This work was funded by the Austrian Science Fund (P33562-B) to KN, and the fellowships of the Austrian Society of Hematology and Oncology to NW and KMK.

Appendix A. Supporting information

Supplementary data associated with this article can be found in the online version at doi:10.1016/j.phrs.2026.108087.

Data availability

Data will be made available on request.

References

[1] N.S. Chandel, Lipid metabolism. Cold Spring Harbor perspectives in biology 2021, 2021, 13.
[2] R. Bravo, V. Parra, D. Gatica, A.E. Rodriguez, N. Torrealba, F. Paredes, Z.V. Wang, A. Zorzano, J.A. Hill, E. Jaimovich, A.F. Quest, S. Lavandero, Endoplasmic reticulum and the unfolded protein response: dynamics and metabolic integration, Int. Rev. Cell Mol. Biol. 301 (2013) 215–290.
[3] K. Funai, S.A. Summers, J. Rutter, Reign in the membrane: how common lipids govern mitochondrial function, Curr. Opin. Cell Biol. 63 (2020) 162–173.
[4] M.J. Bueno, V. Jimenez-Renard, S. Samino, J. Capellades, A. Junza, M.L. Lopez-Rodriguez, J. Garcia-Carceles, I. Lopez-Fabuel, J.P. Bolanos, N.S. Chandel, O. Yanes, R. Colomer, M. Quintela-Fandino, Essentiality of fatty acid synthase in the 2d to anchorage-independent growth transition in transforming cells, Nat. Commun. 10 (2019) 5011.
[5] M.J. Bueno, M. Quintela-Fandino, Emerging role of fatty acid synthase in tumor initiation: Implications for cancer prevention, Mol. Cell. Oncol. 7 (2020) 1709389.
[6] L.M. Butler, Y. Perone, J. Dehairs, L.E. Lupien, V. de Laat, A. Talebi, M. Loda, W. B. Kinlaw, J.V. Swinnen, Lipids and cancer: Emerging roles in pathogenesis, diagnosis and therapeutic intervention, Adv. Drug Deliv. Rev. 159 (2020) 245–293.
[7] A. Horiguchi, T. Asano, T. Asano, K. Ito, M. Sumitomo, M. Hayakawa, Fatty acid synthase over expression is an indicator of tumor aggressiveness and poor prognosis in renal cell carcinoma, J. Urol. 180 (2008) 1137–1140.
[8] T. Puig, C. Turrado, B. Benhamu, H. Aguilar, J. Relat, S. Ortega-Gutierrez, G. Casals, P.F. Marrero, A. Urruticoechea, D. Haro, M.L. Lopez-Rodriguez, R. Colomer, Novel inhibitors of fatty acid synthase with anticancer activity, Clinical cancer research official journal American Association Cancer Research 15 (2009) 7608–7615.
[9] J. Drury, P.G. Rychahou, D. He, N. Jafari, C. Wang, E.Y. Lee, H.L. Weiss, B. M. Evers, Y.Y. Zaytseva, Inhibition of fatty acid synthase upregulates expression of cd36 to sustain proliferation of colorectal cancer cells, Front. Oncol. 10 (2020) 1185.
[10] P.V. Nuzzo, S. Rodrigues, C.F. Ribeiro, I.F. Teixeira, G.N. Fanelli, S. Bleve, F. Ravera, H. Pakula, F. Pederzoli, D.M. Nanus, M. Loda, Targeting cancer metabolism: Therapeutic potential of the fatty acid synthase (fasn) inhibitors, Crit. Rev. Oncol. /Hematol. 214 (2025) 104910.
[11] K. Tomek, R. Wagner, F. Varga, C.F. Singer, H. Karlic, T.W. Grunt, Blockade of fatty acid synthase induces ubiquitination and degradation of phosphoinositide-3-kinase signaling proteins in ovarian cancer, Molecular cancer research MCR 9 (2011) 1767–1779.
[12] T. Puig, H. Aguilar, S. Cufi, G. Oliveras, C. Turrado, S. Ortega-Gutierrez, B. Benhamu, M.L. Lopez-Rodriguez, A. Urruticoechea, R. Colomer, A novel inhibitor of fatty acid synthase shows activity against her2+ breast cancer xenografts and is active in anti-her2 drug-resistant cell lines, Breast cancer research BCR 13 (2011) R131.
[13] C.T. Guy, R.D. Cardiff, W.J. Muller, Induction of mammary tumors by expression of polyomavirus middle t oncogene: A transgenic mouse model for metastatic disease, Mol. Cell. Biol. 12 (1992) 954–961.
[14] L. Jin, D. Li, G.N. Alesi, J. Fan, H.B. Kang, Z. Lu, T.J. Boggon, P. Jin, H. Yi, E. R. Wright, D. Duong, N.T. Seyfried, R. Egnatchik, R.J. DeBerardinis, K. R. Magliocca, C. He, M.L. Arellano, H.J. Khoury, D.M. Shin, F.R. Khuri, S. Kang, Glutamate dehydrogenase 1 signals through antioxidant glutathione peroxidase 1 to regulate redox homeostasis and tumor growth, Cancer Cell 27 (2015) 257–270.
[15] M. Canal, J. Romani-Aumedes, N. Martin-Flores, V. Perez-Fernandez, C. Malagelada, Rtp801/redd1: A stress coping regulator that turns into a troublemaker in neurodegenerative disorders, Front. Cell. Neurosci. 8 (2014) 313.
[16] M.L. Whitney, L.S. Jefferson, S.R. Kimball, Atf4 is necessary and sufficient for er stress-induced upregulation of redd1 expression, Biochem. Biophys. Res. Commun. 379 (2009) 451–455.
[17] G.H. Fong, K. Takeda, Role and regulation of prolyl hydroxylase domain proteins, Cell death Differ. 15 (2008) 635–641.
[18] A. King, M.A. Selak, E. Gottlieb, Succinate dehydrogenase and fumarate hydratase: Linking mitochondrial dysfunction and cancer, Oncogene 25 (2006) 4675–4682.
[19] F. Yu, S.B. White, Q. Zhao, F.S. Lee, Hif-1alpha binding to vhl is regulated by stimulus-sensitive proline hydroxylation, Proc. Natl. Acad. Sci. USA 98 (2001) 9630–9635.
[20] A.B. Bandara, J.C. Drake, D.A. Brown, Complex ii subunit sdhd is critical for cell growth and metabolism, which can be partially restored with a synthetic ubiquinone analog, BMC Mol. Cell Biol. 22 (2021) 35.
[21] R.J. Wedan, J.Z. Longenecker, S.M. Nowinski, Mitochondrial fatty acid synthesis is an emergent central regulator of mammalian oxidative metabolism, Cell Metab. 36 (2024) 36–47.
[22] S.M. Nowinski, A. Solmonson, S.F. Rusin, J.A. Maschek, C.L. Bensard, S. Fogarty, M.Y. Jeong, S. Lettlova, J.A. Berg, J.T. Morgan, Y. Ouyang, B.C. Naylor, J.A. Paulo, K. Funai, J.E. Cox, S.P. Gygi, D.R. Winge, R.J. DeBerardinis, J. Rutter, Mitochondrial fatty acid synthesis coordinates oxidative metabolism in mammalian mitochondria, eLife 9 (2020).
[23] R. Wagner, G. Stubiger, D. Veigel, M. Wuczkowski, P. Lanzerstorfer, J. Weghuber, E. Karteris, K. Nowikovsky, N. Wilfinger-Lutz, C.F. Singer, R. Colomer, B. Benhamu, M.L. Lopez-Rodriguez, P. Valent, T.W. Grunt, Multi-level suppression of receptor-pi3k-mtorc1 by fatty acid synthase inhibitors is crucial for their efficacy against ovarian cancer cells, Oncotarget 8 (2017) 11600–11613.
[24] Y. Liu, Y. Pang, B. Zhu, O. Uher, V. Caisova, T.T. Huynh, D. Taieb, K. Hadrava Vanova, H.K. Ghayee, J. Neuzil, M. Levine, C. Yang, K. Pacak, Therapeutic targeting of sdhb-mutated pheochromocytoma/paraganglioma with pharmacologic ascorbic acid, Clinical Cancer Res. Official J. Am. Assoc. Cancer Res. 26 (2020) 3868–3880.
[25] H. Yoshida, T. Matsui, A. Yamamoto, T. Okada, K. Mori, Xbp1 mrna is induced by atf6 and spliced by ire1 in response to er stress to produce a highly active transcription factor, Cell 107 (2001) 881–891.
[26] D. Feng, A. Witkowski, S. Smith, Down-regulation of mitochondrial acyl carrier protein in mammalian cells compromises protein lipoylation and respiratory complex i and results in cell death, J. Biol. Chem. 284 (2009) 11436–11445.

[27] Y.F. Her, L.J. Maher, 3rd. Succinate dehydrogenase loss in familial paraganglioma: biochemistry, genetics, and epigenetics, Int. J. Endocrinol. 2015 (2015) 296167.
[28] E. Rapizzi, T. Ercolino, R. Fucci, B. Zampetti, R. Felici, D. Guasti, A. Morandi, E. Giannoni, V. Giache, D. Bani, A. Chiarugi, M. Mannelli, Succinate dehydrogenase subunit b mutations modify human neuroblastoma cell metabolism and proliferation, Horm. Cancer 5 (2014) 174–184.
[29] N. Saxena, N. Maio, D.R. Crooks, C.J. Ricketts, Y. Yang, M.H. Wei, T.W. Fan, A. N. Lane, C. Sourbier, A. Singh, J.K. Killian, P.S. Meltzer, C.D. Vocke, T.A. Rouault, W.M. Linehan, Sdhb-deficient cancers: The role of mutations that impair iron sulfur cluster delivery, J. Natl. Cancer Inst. 108 (2016).
[30] P. Navarro, M.J. Bueno, I. Zagorac, T. Mondejar, J. Sanchez, S. Mouron, J. Munoz, G. Gomez-Lopez, V. Jimenez-Renard, F. Mulero, N.S. Chandel, M. Quintela-Fandino, Targeting tumor mitochondrial metabolism overcomes resistance to antiangiogenics, Cell Rep. 15 (2016) 2705–2718.
[31] F.A. Rossato, K.G. Zecchin, P.G. La Guardia, R.M. Ortega, L.C. Alberici, R.A. Costa, R.R. Catharino, E. Graner, R.F. Castilho, A.E. Vercesi, Fatty acid synthase inhibitors induce apoptosis in non-tumorigenic melan-a cells associated with inhibition of mitochondrial respiration, PloS One 9 (2014) e101060.
[32] M. Schreurs, F. Kuipers, F.R. van der Leij, Regulatory enzymes of mitochondrial beta-oxidation as targets for treatment of the metabolic syndrome, Obes. Rev. Off. J. Int. Assoc. Study Obes. 11 (2010) 380–388.
[33] J. Lavie, H. De Belvalet, S. Sonon, A.M. Ion, E. Dumon, S. Melser, D. Lacombe, J. W. Dupuy, C. Lalou, G. Benard, Ubiquitin-dependent degradation of mitochondrial proteins regulates energy metabolism, Cell Rep. 23 (2018) 2852–2863.
[34] Z. Qian, Y. Jiang, Y. Cai, E. Gao, C. Wang, J. Dong, F. Wang, L. Liu, D. Wu, F. Zhang, Y. Wang, X. Ning, Q. Li, Y. You, Y. Gu, J. Mei, X. Zhao, Y. Zhang, Fasn inhibits ferroptosis in breast cancer via usp5 palmitoylation-dependent regulation of gpx4 deubiquitination, Journal experimental clinical cancer research CR 44 (2025) 289.
[35] S.P. Burr, A.S. Costa, G.L. Grice, R.T. Timms, I.T. Lobb, P. Freisinger, R.B. Dodd, G. Dougan, P.J. Lehner, C. Frezza, J.A. Nathan, Mitochondrial protein lipoylation and the 2-oxoglutarate dehydrogenase complex controls hif1alpha stability in aerobic conditions, Cell Metab. 24 (2016) 740–752.
[36] J. Goncalves, S. Moog, A. Morin, G. Gentric, S. Muller, A.P. Morrell, K. Kluckova, T. J. Stewart, C.L. Andoniadou, C. Lussey-Lepoutre, P. Benit, A. Thakker, L. Vettore, J. Roberts, R. Rodriguez, F. Mechta-Grigoriou, A.P. Gimenez-Roqueplo, E. Letouze, D.A. Tennant, J. Favier, Loss of sdhb promotes dysregulated iron homeostasis, oxidative stress, and sensitivity to ascorbate, Cancer Res. 81 (2021) 3480–3494.
[37] K.A. Janeway, S.Y. Kim, M. Lodish, V. Nosé, P. Rustin, J. Gaal, P.L.M. Dahia, B. Liegl, E.R. Ball, M. Raygada, A.H. Lai, L. Kelly, J.L. Hornick, N.P.W.T.G. Clinic, M. O'Sullivan, R.R. de Krijger, W.N.M. Dinjens, G.D. Demetri, C.R. Antonescu, J. A. Fletcher, L. Helman, C.A. Stratakis, Defects in succinate dehydrogenase in gastrointestinal stromal tumors lacking and mutations, Proc. Natl. Acad. Sci. USA 108 (2011) 314–318.
[38] Y. Ni, K.M. Zbuk, T. Sadler, A. Patocs, G. Lobo, E. Edelman, P. Platzer, M.S. Orloff, K.A. Waite, C. Eng, Germline mutations and variants in the succinate dehydrogenase genes in cowden and cowden-like syndromes, Am. J. Hum. Genet. 83 (2008) 261–268.
[39] S. Vanharanta, M. Buchta, S.R. McWhinney, S.K. Virta, M. Peczkowska, C. D. Morrison, R. Lehtonen, A. Januszewicz, H. Jarvinen, M. Juhola, J.P. Mecklin, E. Pukkala, R. Herva, M. Kiuru, N.N. Nupponen, L.A. Aaltonen, H.P. Neumann, C. Eng, Early-onset renal cell carcinoma as a novel extraparaganglial component of sdhb-associated heritable paraganglioma, Am. J. Hum. Genet. 74 (2004) 153–159.
[40] P.P. Aspuria, S.Y. Lunt, L. Varemo, L. Vergnes, M. Gozo, J.A. Beach, B. Salumbides, K. Reue, W.R. Wiedemeyer, J. Nielsen, B.Y. Karlan, S. Orsulic, Succinate dehydrogenase inhibition leads to epithelial-mesenchymal transition and reprogrammed carbon metabolism, Cancer Metab. 2 (2014) 21.
[41] K. Hadrava Vanova, C. Yang, L. Meuter, J. Neuzil, K. Pacak, Reactive oxygen species: A promising therapeutic target for sdhx-mutated pheochromocytoma and paraganglioma, Cancers 13 (2021).
[42] Y. Saimoto, D. Kusakabe, K. Morimoto, Y. Matsuoka, E. Kozakura, N. Kato, K. Tsunematsu, T. Umeno, T. Kiyotani, S. Matsumoto, M. Tsuji, T. Hirayama, H. Nagasawa, K. Uchida, S. Karasawa, M. Jutanom, K.I. Yamada, Lysosomal lipid peroxidation contributes to ferroptosis induction via lysosomal membrane permeabilization, Nat. Commun. 16 (2025) 3554.
[43] T.W. Grunt, A. Slany, M. Semkova, R. Colomer, M.L. Lopez-Rodriguez, M. Wuczkowski, R. Wagner, C. Gerner, G. Stubiger, Membrane disruption, but not metabolic rewiring, is the key mechanism of anticancer-action of fasn-inhibitors: a multi-omics analysis in ovarian cancer, Sci. Rep. 10 (2020) 14877.
[44] C. Xia, X. Sun, Y. Wang, J. Min, W. Zhang, C. Wei, L. Gao, F. Zhao, A.R. Aleem, W. Peng, Y. Hu, Q. Zhang, C. Fu, Synergistic targeting of fasn and hmgcs1 by cerulenin enhances tumor cell ferroptosis sensitivity through rewiring lipid metabolism and blocking gpx4 biosynthesis, Cancer Lett. 633 (2025) 217992.
[45] N. Wilfinger, S. Austin, B. Scheiber-Mojdehkar, W. Berger, S. Reipert, M. Praschberger, J. Paur, R. Trondl, B.K. Keppler, C.C. Zielinski, K. Nowikovsky, Novel p53-dependent anticancer strategy by targeting iron signaling and bnip3l-induced mitophagy, Oncotarget 7 (2016) 1242–1261.
[46] C. Turrado, T. Puig, J. Garcia-Carceles, M. Artola, B. Benhamu, S. Ortega-Gutierrez, J. Relat, G. Oliveras, A. Blancafort, D. Haro, P.F. Marrero, R. Colomer, M.L. Lopez-Rodriguez, New synthetic inhibitors of fatty acid synthase with anticancer activity, J. Med. Chem. 55 (2012) 5013–5023.
[47] J.A. Menendez, I. Mehmi, E. Atlas, R. Colomer, R. Lupu, Novel signaling molecules implicated in tumor-associated fatty acid synthase-dependent breast cancer cell proliferation and survival: Role of exogenous dietary fatty acids, p53-p21waf1/cip1, erk1/2 mapk, p27kip1, brca1, and nf-kappab, Int. J. Oncol. 24 (2004) 591–608.
[48] D. Botman, W. Tigchelaar, C.J. Van Noorden, Determination of glutamate dehydrogenase activity and its kinetics in mouse tissues using metabolic mapping (quantitative enzyme histochemistry), J. Histochem. Cytochem. Official J. Histochem. Soc. 62 (2014) 802–812.
[49] L. Guo, A.A. Shestov, A.J. Worth, K. Nath, D.S. Nelson, D.B. Leeper, J.D. Glickson, I. A. Blair, Inhibition of mitochondrial complex ii by the anticancer agent lonidamine, J. Biol. Chem. 291 (2016) 42–57.
[50] C.J.F. Van Noorden, W.M. Frederiks. Enzyme histochemistry: a laboratory manual of current methods, Oxford University Press/Royal Microscopical Society, 1992.
[51] A. Miller, C. Nagy, B. Knapp, J. Laengle, E. Ponweiser, M. Groeger, P. Starkl, M. Bergmann, O. Wagner, A. Haschemi, Exploring metabolic configurations of single cells within complex tissue microenvironments, Cell metabolism 26 (2017) 788–800, e786.
[52] C. Frezza, S. Cipolat, L. Scorrano, Organelle isolation: Functional mitochondria from mouse liver, muscle and cultured fibroblasts, Nat. Protoc. 2 (2007) 287–295.
[53] K. Dettmer, N. Nurnberger, H. Kaspar, M.A. Gruber, M.F. Almstetter, P.J. Oefner, Metabolite extraction from adherently growing mammalian cells for metabolomics studies: Optimization of harvesting and extraction protocols, Anal. Bioanal. Chem. 399 (2011) 1127–1139.